RIVISTA DEL NUOVO CIMENTO Vol. 36, N. 8 2013
DOI 10.1393/ncr/i2013-10091-2

The weak neutral current—discovery and impact(*)

D. Haidt(1) and A. Pullia(2)

(1) *Emeritus of DESY - Hamburg, Germany*
(2) *Dipartimento di Fisica, Università di Milano-Bicocca e INFN, Sezione di Milano Milano, Italy*

ricevuto il 14 Maggio 2013

Summary. — This review describes the discovery of weak neutral currents in Gargamelle, the determination of their properties and their impact during the past 40 years.

PACS 12.15.Mm – Neutral currents.
PACS 13.15.+g – Neutrino interactions.
PACS 12.15.-y – Electroweak interactions.
PACS 13.66.Jn – Precision measurements in e^+e^- interactions.

(*) Based on talks presented at the Congress of the Italian Physical Society at L'Aquila on the occasion of the conferment of the *Enrico Fermi award* on September 26, 2011.

1. Introduction

The Italian Physical Society has devoted in 2011 the prestigious *Enrico Fermi Prize* to honor the discovery of weak neutral currents. This prompted a look back at the discovery and the great achievements since then.

Enrico Fermi is the father of weak interactions. Immediately after the Solvay Congress in autumn 1933 Fermi combined Pauli's neutrino hypothesis and the just discovered neutron interpreted as elementary particle rather than a composite of a proton with an electron. He conceived the nuclear β-decay as the transition between the nuclear states mediated by the emission of a (νe)-pair, in analogy to the emission of a photon in an atomic radiative decay, and published the final work 1934 under the title *Versuch einer Theorie der β-Strahlen* [1]. Seen from today the year 1973, when the weak neutral currents were discovered, lies just in the middle. In the period until the end of the 1950s Fermi's theory achieved the elegant formulation as $V - A$ theory. It successfully described all the low-energy weak-interaction data, mainly decays, but serious theoretical problems occurred when facing the high-energy behaviour. In the next decade new theoretical ideas on local gauge theories, spontaneous symmetry breaking and renomalizability resulted in the Glashow-Salam-Weinberg model. It incorporated the known weak and electromagnetic interactions mediated by the weak charged vector boson $W^{\pm}$ (then not yet discovered) and the photon. In addition to the charged vector boson also a neutral vector boson Z was postulated, which would give rise to weak neutral-current processes, such as $\nu p \to \nu p$. In the mean time new experimental tools became available: proton synchrotrons, neutrino beams in the GeV region and large detectors.

Gargamelle was ready to take up the challenge in 1972 and the year later the discovery of a new type of interaction could be claimed. It was interpreted as the occurrence of weak neutral currents. From then up to date the large laboratories started an intense and systematic scientific program to study the properties of weak neutral currents. During these years the neutrino experiments reached high precision despite their notorious low cross sections. Even in elastic neutrino electron scattering samples with a thousand events were obtained. With PETRA and PEP the electroweak interference was tested at time-like momenta squared of order $1000\,\mathrm{GeV}^2$. Really precise tests were achieved at the e^+e^- colliders LEP and SLC and at the $p\overline{p}$ colliders at CERN and Fermilab. Recently a new phase was initiated with the Large Hadron Collider (LHC) aiming at pinning down the Higgs sector and exploring the 1 TeV energy regime.

The review describes in sect. **2** the discovery of weak neutral currents. The discovery has been the subject of several symposia, see for instance [2-5]. Section **3** outlines the electroweak theory, followed by a broad selection of relevant experimenal results. The last section summarizes the impact of the discovery of weak neutral currents to particle physics and other fields.

2. – The discovery

The idea to build a large heavy liquid bubble chamber goes back to the Siena conference 1963, where the results from the first neutrino experiments have been presented, among them the 1.2 m heavy liquid bubble chamber (the Ramm chamber) and the spark chamber operated in the neutrino beam derived from the CERN Proton Synchrotron (PS). The new energy regime of 1–10 GeV was opened [6] and represented a huge step in energy compared to the previous studies in nuclear or particle decays. On the solid basis of the $V - A$ theory T. D. Lee [7] has established a catalog of questions and some of them were addressed immediately, in particular searches for the carrier of the weak force, for two neutrino species and the existence of weak neutral currents. With the rich program in mind Lagarrigue, Rousset and Musset thought of a second-generation bubble chamber about an order of magnitude larger in size. The aim was to augment the event samples in number and quality. The best choice was therefore to fill the chamber with a heavy liquid.

The physics program was discussed in a two day meeting at Milan in fall 1968. The search for the intermediate vector boson $W^{\pm}$ was considered of highest priority. However, the just discovered substructure of the proton at SLAC attracted high attention and inspired the exploration of the nucleon by the weak current, *i.e.* with the weak intermediate vector boson in analogy to the photon in *ep* scattering. Apart from exposing the chamber to neutrino beams also hadron beams were considered. What was not discussed, was the question of whether *weak neutral currents* existed. The proposal [8] was submitted in 1970 and the commissioning of the chamber started at the end of 1970. Figure 1 illustrates the assembly of Gargamelle. In the following years Gargamelle was operated in both neutrino and antineutrino beams at the CERN PS and shortly at the CERN SPS until 1978, when the chamber broke down.

Seven laboratories shared the film for scanning and measuring. This meant to adopt strict scanning rules in order to ensure consistent event samples. The experience gained in the previous neutrino experiments with the Ramm 1.2 m chamber served to set up the rules. Events were attributed to different classes. The *class A* contained events with a muon candidate, for neutrino data negatively and for antineutrino data positively charged, while *class B* contained events with final-state particles identified as

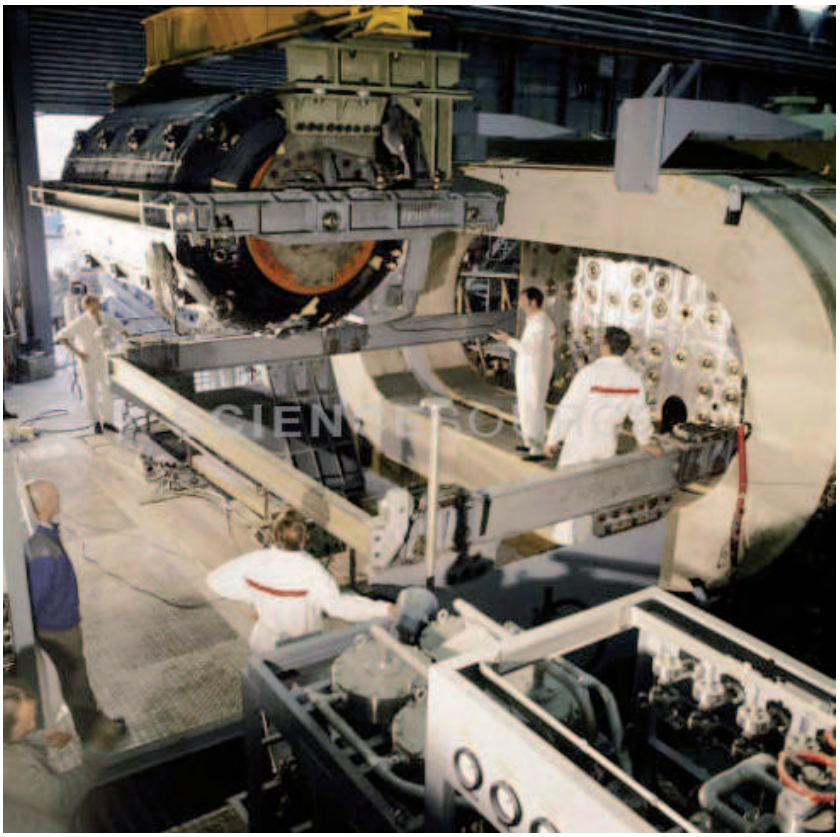

Fig. 1. – Installation of the Gargamelle chamber body into the coils.

hadrons, *i.e.* definitely no muon. The events in *class B* were called the n^* events, since they were supposed to consist of neutron-induced interactions in the chamber. Such neutrons unavoidably arose as secondaries of neutrino interactions upstream in the shielding (cf. fig. 3). These events with surely identified final-state hadrons served the purpose to estimate how many charged hadrons fake a muon candidate([1]). As soon as the quest for weak neutral currents came up, the *class B* turned out to be of crucial importance. Two other classes were *class C* containing interactions with low-energy protons and *class D* containing just isolated electrons.

The initial thrust was to gather a large sample of inelastic neutrino and antineutrino events to study the partonic structure of the nucleon. However, the theoretical developments during the 1960s, which resulted in a renormalizable model for weak and electromagnetic phenomena, eventually alerted the Gargamelle group. This model postulated the existence of weak neutral currents. Gargamelle met the challenge to search for such phenomena. Infact, the *class B per definitionem* would already contain neutral-current candidates, if they really existed. An encouraging first indication came from a

([1]) Years later electronic devices were added to bubble chambers in order to identify muons; before the discovery of weak neutral currents the above method was adequate.

TABLE I. – *The NC and CC event samples in the ν and $\overline{\nu}$ films.*

Event type	ν-exposure	$\overline{\nu}$-exposure
# NC	102	64
# CC	428	148

study performed by Pullia and the group of Milan [2]. He looked at the vertex distribution along the chamber of *class B* events and found it rather flat, thus untypical for neutron interactions. A dedicated investigation was then initiated in spring 1972 and a special group for the search of neutral currents was formed.

A neutral-current candidate was defined as an event within the fiducial volume consisting of only identified hadrons and having a visible energy in excess of 1 GeV. The strong energy cut was imposed in order to reduce the expected low-energy neutron background. The scanning and measuring resulted within one year in sizeable event samples (see table I). In order to judge the features of the neutral-current candidates charged-current events served as control sample after imposing the same criteria on the hadronic final state and ignoring the presence of a muon candidate.

Great excitement arose in december 1972, when an isolated electron was observed in the antineutrino film (see sect. **4**˙2). The obvious explanation by the conventional charged-current process $\nu_e p \to e^- +$ *invisible hadrons* could be excluded, while the candidate was readily interpreted as a purely leptonic weak neutral-current process $\overline{\nu}_\mu e^- \to \overline{\nu}_\mu e^-$ and provided the first evidence for weak neutral currents. This event and the big number of neutral-current candidates in both the neutrino and the antineutrino films (see table I) created an euphoric meeting of the collaboration in spring 1973. From the experience gained in the previous neutrino experiments with the 1.2 m heavy liquid bubble chamber (the Ramm chamber) it was clear that the real challenge consisted in proving that these candidates were not simply due to neutron interactions. In an intense effort in the coming four months the problem was tackled (see details in the next section). At the end of long and thorough discussions the collaboration was convinced that indeed the neutrons contribute only a small fraction to the event sample, thus the existence of a new effect could be claimed. The result was presented by Musset at the end of July 1973 in the CERN Auditorium and shortly later, on July 25, the paper entitled *Observation of neutrino-like interactions without muon or electron in the Gargamelle neutrino experiment* was sent for publication to *Physics Letters* [9]. The paper on the isolated electron [10] had already been sent for publication at the beginning of the month.

2˙1. *Neutron background*. – At the collaboration meeting in March 1973 the results of the search for weak neutral currents were discussed and three arguments seemed to indicate that their discovery was imminent. First, the number of candidates was large and on the same order of magnitude as the charged-current reference sample (cf. table I). Second, the spatial distributions of the neutral-current candidates (cf. fig. 2) is untypical for being neutron-induced, otherwise entering neutrons should show up as an exponential falloff with their characteristic interaction length in the liquid freon (CF_3Br), which is short compared to the dimensions of the chamber. Third, the spatial distribution is characteristic of events induced by neutrinos, since their distribution is nearly flat over

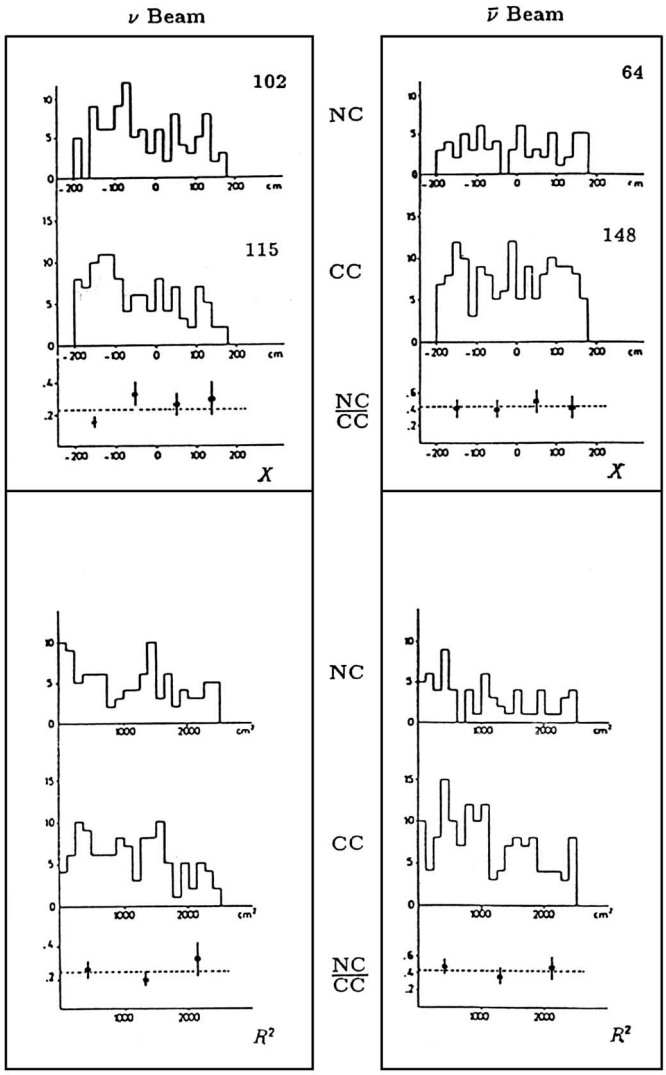

Fig. 2. – Spatial distributions of the neutral- and charged-current candidates. X is the longitudinal vertex position of the events, R the radial position.

the full longitudinal extention of the chamber, in particular there are many events in the downstream part of the chamber, where neutrons should not contribute anymore. Furthermore, all distributions of the neutral-current sample are similar in shape to the charged-current reference sample.

Yet, the euphorism was damped, when Fry and Haidt [14] put forward two counter-arguments. A look at the experimental setup (see figs. 1 and 3) shows that the chamber is surrounded by heavy material. Since the neutrino beam is not limited to the dimension of the chamber front window, but has a broad lateral profile, there is a huge number of neutrino interactions in the surrounding material. All these neutrino interactions act as sources of neutrons with the consequence that neutrons do not only enter at the chamber

front window, but also all along the chamber and thus generate a flat longitudinal distribution just as expected for genuine neutrino-induced interactions. The other argument concerned the fact that an entering neutron may be the result of a *hadron cascade*. Any final-state hadron of a neutrino interaction generates a cascade. What is observed in the chamber, is the *end* of the cascade. Therefore, the neutron (strictly speaking neutral hadron) entering the chamber and depositing more than 1 GeV may be the result of a two- or more-step hadron cascade. The net effect is that the neutron background is proportional to the cascade length, rather than to the interaction length, and may be dangerously larger than anticipated. In conclusion, the above three qualitative arguments proved not to be stringent and it was premature to make any claim.

The collaboration felt the responsability to come up with a clear-cut statement as to whether weak neutral currents existed or not. It was then imperative to carry out a quantitative estimate of the neutron background and to decide eventually between the two cases

$$\#n \ll \#\mathrm{NC} \qquad \text{or} \qquad \#n \approx \#\mathrm{NC}.$$

On the other hand, it was equally imperative to be fast and not to lose time.

2˙1.1. The quantitative estimate. The goal was to calculate the absolute number of neutron-induced events in the neutral-current candidate sample (a detailed account may be found in ref. [15]). The description of the problem indicates four essential ingredients for the neutron background calculation:

a) Geometry and matter distribution:
Figure 3 shows the experimental setup. The interior of the chamber Gargamelle is viewed by 8 optical cameras and is divided in three cylindrical volumes. The innermost volume is the fiducial volume with a radius of 50 cm and longitudinal extention of 4 m. It is surrounded by the visible volume extending in radius up to 75 cm, while the outermost volume of the liquid in radius from 75 to 100 cm is invisible. The chamber liquid consists of heavy freon with the chemical composition CF_3Br and density of $1.5\,\mathrm{g/cm^3}$ ensuring a large target mass, thus large event numbers, and also a high efficiency for identifying final state hadrons. In particular, the apparent interaction length of neutrons was about 80 cm and the radiation length of photons 11 cm. A final-state muon, μ^- in neutrino interactions and a μ^+ in antineutrino interactions, appeared as a track in the chamber and usually left the chamber. A charged pion simulated a muon, unless identified through a visible strong interaction. For that reason candidates for $\nu + N \to \mu + \mathit{anything}$ had to be corrected for faking pions and this was the original purpose for the category B. The definition of the event categories was made long before the search for neutral currents. It was then a happy circumstance, that the new type of events should already be part of the category B. The chamber body consisted of steel, a good fraction of an interaction length thick. In front of the chamber was the neutrino shielding made of iron. The chamber was imbedded in huge magnetic coils.

b) Neutrino beam:
The precise knowledge of the neutrino flux was an essential part of the whole neutrino program. In a separate experiment 1970 using the Allaby spectrometer [16, 17] the CERN PS proton beam of 24 GeV was hitting cylindical targets ranging from beryllium up to tungsten and served to measure the secondary $\pi^\pm$, $K^\pm$, p and

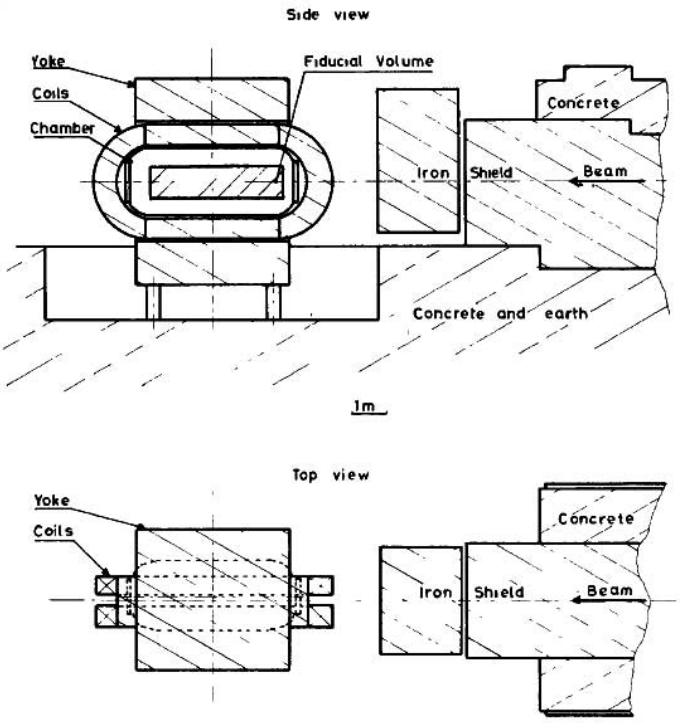

Fig. 3. – Top and side view of the experimental setup. The neutrino beam enters from the right through the iron shielding. The body of the chamber inside the magnet coil and yoke is illustrated together with the fiducial volume corresponding to about $3\,\mathrm{m}^3$.

$\overline{p}$ with respect to momentum and angle. With this experimental input the fluxes of neutrinos and muons coming from the meson decays in flight could be predicted. A strong constraint was obtained by comparing the predicted muon flux and the measured muon flux by special muon detectors distributed all over the neutrino shielding [18].

c) Final-state properties:
The neutrino-induced events provided directly the properties of the final hadron state.

d) Cascade:
The real challenge was to find a way how to handle the evolution of the final hadron state.

Given the complexity of the problem the appropriate approach to carry out the task was to apply Monte Carlo methods. The program code was structured in modular form. In this way it was possible to incorporate immediately the gross features, before all aspects were worked out in more detail. Also easy access to the critical parts was assured for investigating *ad hoc* hypotheses. This turned out to be valuable, when the stability of the predictions was later on discussed.

The representation of the geometry and density distributions of the experimental setup was hard work, but straightforward. The neutrino flux was known and readily

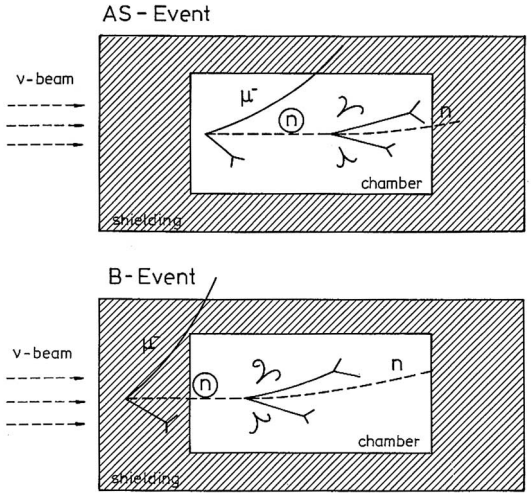

Fig. 4. – Sketch of the two configurations of a neutron in the detector.

incorporated. The dynamics of neutrino interactions, *i.e.* the energy and angular distributions of the final-state particles were obtained from the data themselves. The only difficult part was how to treat the propagation of the neutrino reaction products. It looked almost hopeless at first to develop from scratch within a few months the appropriate code for a multi-branch shower, until it was realized [14] that final-state mesons are never energetic enough to produce a neutron depositing more than 1 GeV, when entering in the fiducial volume of the chamber. The even stronger conclusion could be drawn that the cascade is linear and transported only by fast nucleons. The propagation of the nucleon cascade depended therefore essentially on a single distribution, the *elasticity* distribution, determining at each interaction point which fraction of the initial energy is carried away by the secondary nucleon. In the shieding it does not matter whether a fast proton or a fast neutron is carrying the cascade, only in the last step it must be a neutron leaving the shielding and entering the chamber. The effective interaction length of fast nucleons in the iron shielding is about 17 cm, however the cascade length may be much longer depending on the energy of the initial nucleon and the elasticity at each cascade step. The published data on proton-proton and proton-nuclei interactions were sufficient to derive the shape of the elasticity distribution. In July 1973, four months after the spring meeting of the collaboration, the neutron background program was elaborated in detail and was ready for predicting the absolute number of neutrons simulating neutral-current candidates.

The nucleon cascade is observable in the chamber in two configurations, namely as its *end*, if initiated in the shielding, or as its *beginning*, if initiated in the chamber, as sketched in fig. 4 [15]. These two configurations were denoted as B-events and AS-events, standing for *background* and *associated* events, and have been predicted by the neutron background program. From the calculated ratio B/AS and the observed number of AS events it was then possible to predict the absolute number of B events.

As a first application the hypothesis *All neutral-current candidates are neutron-induced* was considered. Under this worst-case-hypothesis the number of neutron-induced events is maximal, namely #B = #NC, thus 102 in the ν-film and 64 in the $\overline{\nu}$-film, accord-

ing to table I. Furthermore, the event sample fixed the energy and angular distributions. The predicted B/AS ratio turned out to be 1 ± 0.3. With the observed number of associated events, 15 in the ν-film and 12 in the $\overline{\nu}$-film, the predicted number of background events was then 15 and 12 in violent contradiction to the actually observed number of events 102 and 64. Therefore, the hypothesis had to be rejected with the conclusion that, on the contrary, the observed number of neutral-current candidates was not dominated by neutron-induced events.

For a realistic estimation of the neutron-induced background the above assumed energy and angular distributions had to be replaced by distributions appropriate for neutrons emitted in neutrino interactions. Then, the resulting ratio B/AS decreased to 0.7 with an estimated 30% systematic uncertainty. The fact that a ratio is predicted reduced uncertainties related to some of the input distributions. The really critical part concerned the properties of the cascade, which however were well established by published strong interaction data. The neutron background prediction was parameter-free and proved that the observed neutral-current candidates represent a genuine new effect. This conclusion was reached during the month of July 1973 and the paper claiming neutrino-induced muonless events with hadrons [9] was sent at the end of July 1973 to *Physics Letters* for publication.

Intense discussions inside the collaboration preceded the last weeks of July until everybody was convinced of a discovery. No argument against the existence of a new effect remained without convincing answer. It was in these circumstances that the flexibility of the neutron background program proved its value. It was easy to change *ad hoc* any aspect of the calculation and to illustrate right away the implications. Even extreme arguments have been proposed and afterwards rejected because of internal inconsistencies. These severe internal discussions anticipated the attacks put forward against Gargamelle later on by the comunity.

The B/AS method was applied in various later analyses in Gargamelle and BEBC.

2˙1.2. Internal method. Another important piece of information was the actual position of the events within the chamber [11, 34, 22]. The interaction lengths of neutrinos as opposed to neutrons in the chamber liquid is widely different. The aim was to investigate the apparent interaction length of the NC samples and to find out whether it was neutrino-like or neutron-like [33]. To this end the flight path l and the potential path L of each event are combined to form the quantity

$$v = \frac{1 - e^{-l/\lambda}}{1 - e^{-L/\lambda}}\,, \tag{1}$$

suggested and used by Pullia, where the potential path L is the maximum path in the fiducial volume guaranteeing identification of the hadrons in the final state. The interaction length λ is obtained as the best value of the distribution $T(v)$. The direction of flight was estimated event by event from the total visible momentum of the final hadron state and the same procedure was followed by the use of the hadronic part of the charged current events. This method does not require any information coming from the outside of the chamber. The results for the various event samples are collected in table II and illustrated in fig. 5. As expected the apparent interaction length of genuine neutrinos, available in the CC samples, is consistent with infinity.

The apparent interaction length of the events in the NC event sample is smaller by an amount which depends on the size of the neutron background. The sample of *associated*

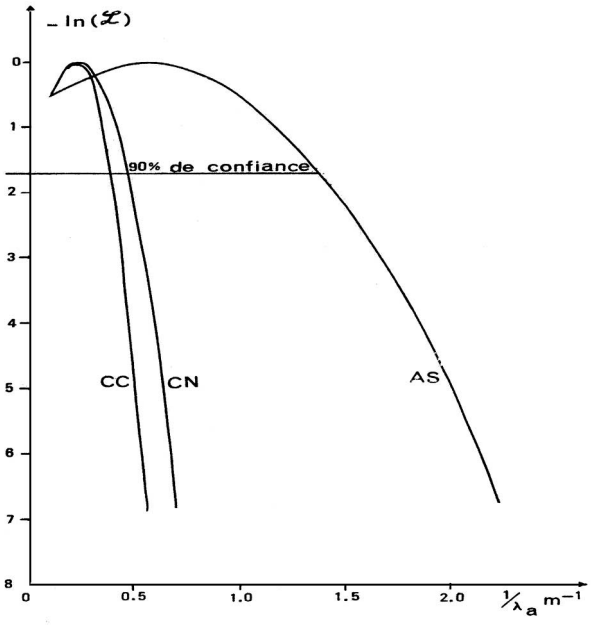

Fig. 5. – Log likelihood distributions of charged current (CC), neutral current (CN) and associated (AS) events. The horizontal line indicates the 90% confidence level.

events (AS), *i.e.* events with a neutron interaction originating from an upstream neutrino interaction provided a direct measurement of the apparent neutron interaction length in the chamber liquid. Further information about neutrons came from a study of those generated within proton-induced cascades in Gargamelle itself (cf. sect. **2**˙3). Proton interactions are representative of neutron interactions, since by charge exchange they are expected to behave similarly to neutrons in the Gargamelle liquid, which has about an equal amount of protons and neutrons. The distribution T_n of the quantity v with

TABLE II. – *Interaction lengths of NC, CC event obtained from the likelihood analysis.*

Beam	$1/\lambda$ for NC	$1/\lambda$ for CC
ν	$0.16 \pm 0.12\,\mathrm{m}^{-1}$	$0.15 \pm 0.10\,\mathrm{m}^{-1}$
$\overline{\nu}$	$0.27 \pm 0.13\,\mathrm{m}^{-1}$	$0.10 \pm 0.10\,\mathrm{m}^{-1}$

TABLE III. – x = *contribution of neutrinos,* B = *neutron background, MC is the Monte Carlo result for the background.*

Beam	x	$B = 1 - x$	MC Results
ν	$0.85^{+0.08}_{-0.10}$	$(15 \pm 9)\%$	$(11 \pm 5)\%$
$\overline{\nu}$	$0.82^{+0.10}_{-0.14}$	$(18 \pm 12)\%$	$(12 \pm 6)\%$

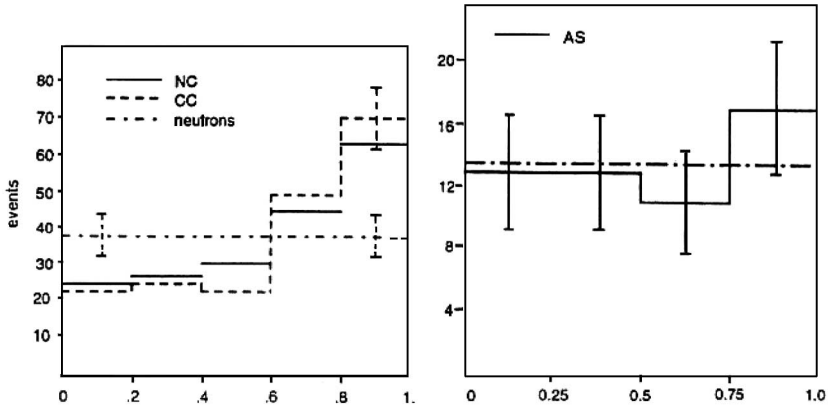

Fig. 6. – Histograms for the variable v for CC and NC (left panel) and histogram of v for AS (right panel).

$\lambda = \lambda_n$ is expected to be flat for a genuine neutron-induced event sample, while the distribution T_ν of this same quantity for genuine neutrino-induced events is expected to increase. This is illustrated in fig. 6. Thus the distribution $T_{\rm NC}(v) = {\rm d}N/{\rm d}v$ of the number N of NC candidates is quantified by

$$T_{\rm NC} = (1 - x)T_n + xT_\nu,$$

where x is the fraction of genuine neutrinos in the neutral-current sample. Assuming $\lambda_n = 0.70\,{\rm m}$ the fit for the fraction x gives $x = 0.85^{+0.08}_{-0.10}$ for neutrinos, while for λ_n increased to 1.0 m the fit value decreases to $0.75^{+0.12}_{-0.18}$.

The net result is that the NC sample consists predominantly of neutrino-induced events in agreement with the result in the subsection above. By using both neutrino and antineutrino NC events and by applying a cut on potential path L ($1.5 < L < 4\,{\rm m}$) as suggested by Haidt [12], the following result was obtained: $(1/\lambda)_{\rm NC} = 0.10 \pm 0.15\,{\rm m}^{-1}$, while the typical value for neutrons is $(1/\lambda)_n = (1.4 - 1.0)\,{\rm m}^{-1}$. In table III [22] are reported all fits obtained for the background (B) in the neutrino and antineutrino case and the comparison with the results obtained by the Monte Carlo calculation.

2˙1.3. Other methods. Rousset [21] has developed a thermodynamic model assuming a homogeneous medium of infinite extention and a uniform neutrino flux density. Neutrons must be in equilibrium with neutrinos. The total number N of neutron interactions equals the sum of B and AS. With α being the fraction of neutrons simulating a NC candidate and $\langle p\rangle$ the probability of detecting a neutron as associated to an upstream neutrino interaction in the chamber the two relations $N = \alpha N_\nu$ and $AS = \alpha N_\nu \langle p\rangle$ hold and the ratio B/AS adopts the form

$$\frac{\rm B}{\rm AS} = \frac{1}{\langle p\rangle} - 1. \tag{2}$$

The probability is given by $p = 1 - \exp(-L/\lambda)$, where L is the potential path for detecting a neutron and λ the apparent interaction length. All the experimental details such as the

radial and energy distributions of the neutrino flux, the characteristics of the neutron cascade, the angular and energy spectrum of the neutrons are contained in the single arbitrary parameter $\langle p \rangle$. For a numerical prediction a value for $\langle p \rangle$ has to be chosen either by guess work or by applying the expectations from the neutron background calculation described above. The simple formula had proven useful in discussions, since it gave quick and qualitative estimates.

With the experience from the earlier experiments in the 1.2 m Ramm chamber with freon and propane, Perkins [20] made in April 1972 an assessment of the chances to discover neutral currents, when the actual search in Gargamelle just started. He counted the number of genuine neutrino events with muon and hadron energy above 1 GeV and estimated from the number associated and unassociated neutral stars the contributing neutron background. The net result was that the fraction 39/289 of the events with muon may be attributed to events without muon. Perkins concluded with a threefold recommendation: i) it is worth performing an in-depth analysis in Gargamelle, ii) the effect may be appreciable and iii) the analysis is full of innumerable pitfalls.

2˙2. *Criticism and final acceptance.* – The discovery of neutrino-induced muonless events was reported to the Electron-Photon Conference at Bonn at the end of August 1973. The Harvard-Pennsylvania-Wisconsin Group (HPW) reported also muonless events observed in a counter experiment (EA1) at the NAL (today Fermi Laboratory) neutrino beam with energies in the 100 GeV regime. In one of the parallel sessions the claim was critically discussed, but at the end of the conference the general belief was that weak neutral currents were discovered. However, a hot summer and fall were to come. Rather soon critical voices started questioning the Gargamelle result and tried to blame for that the treatment of the neutron cascade. They argued that an underestimate of the neutron background would trivially mean the observation of merely neutron interactions. Such arguments were invalidated by the members of Gargamelle stressing the fact, that all aspects of neutron backgound calculation relied on data and were well under control. Nevertheless, the disbelief persisted and even became stronger, when it got known that HPW withdrew the effect in a subsequent run with their modified detector.

2˙3. *The proton experiment.* – The situation for the CERN management became unpleasant to the extent that a special experiment was approved with the aim to dissipate all objections regarding the solidity of the neutron background evaluation or else to reveal a flaw in it. To this end Gargamelle was exposed in two short runs in November (week 45/6) and December (week 50/1) 1973 to single-proton pulses of 4 fixed energies, namely 4, 7, 12, 19 GeV. Gargamelle was filled with the same liquid freon which consisted of a similar number of protons and neutrons justifying the assumption of charge symmetry. In this case the properties of the cascade initiated by the incident protons are representative for neutrons and could be used to test the essential ingredients of the background calculation. The neutron background program was adapted to the conditions of this experiment and used to predict *beforehand* all relevant distributions foreseen as test of the crucial aspects as a function of energy. The runs were evaluated by a small team (Rousset, Pattison, Pomello and Haidt). Definitive and convincing results were ready at the end of March 1974 and were reported by Haidt in April 1974 to the APS Meeting at Washington [19].

The analysis concentrated on three essential issues:

– The apparent interaction length:
  It was obtained by measuring the length of the entering proton track until the first

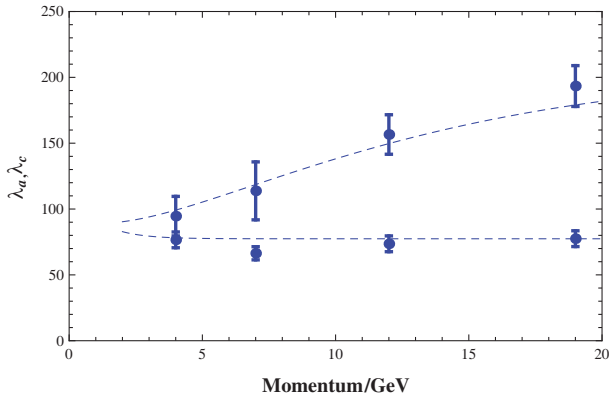

Fig. 7. – The apparent interaction length and the cascade length are shown as a function of the incident proton energy and compared with the prediction of the neutron background program (dashed line).

visible interaction with an energy deposition of at least 150 MeV. The result is shown in fig. 7.

– The cascade length:
It was obtained by measuring the length of the cascade until the last visible interaction with energy deposition of at least 1 GeV, *i.e.* simulating a neutral-current candidate. The result is shown by the upper points and curve of fig. 7.

– The charge exchange rate:
Measurement of the fraction of events consisting after the first interaction of at least one more interaction simulating a neutral-current candidate. Figure 8 shows the fraction as a function of the incident proton energy for the two cases with and without charge exchange.

The agreement of the measured and predicted apparent interaction length in the chamber liquid is a non-trivial test, since the *apparent* interaction length is not calculated from the total cross section, but from that part of the elastic and inelastic cross sections, which lead at the first interaction vertex to a final state with an observable minimum energy (150 MeV), otherwise the neutron would not have been detected as interacting. The shape of the elasticity distribution reflects the quasielastic contribution. Small variations of

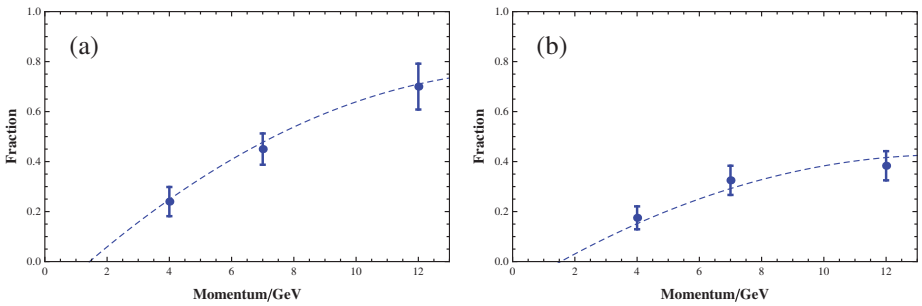

Fig. 8. – a) Fraction of protons interacting more than once and simulating a neutral-current candidate; b) idem, but secondary neutron.

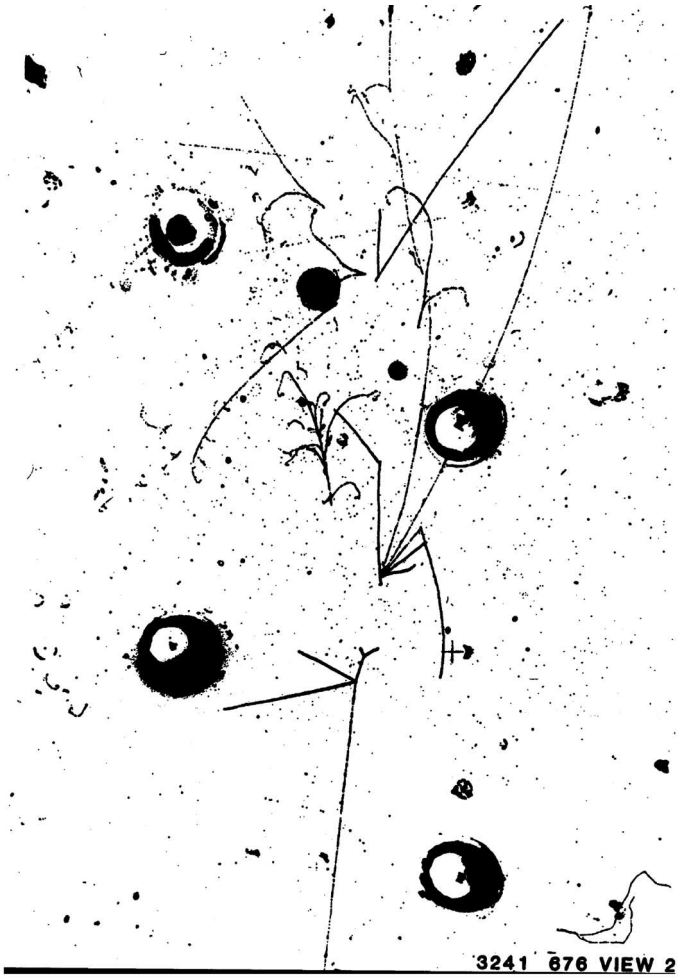

Fig. 9. – Example of a multistep cascade initiated by a 7 GeV proton entering from below in the Gargamelle chamber. After the first interaction a charge exchange occurs and the cascade is continued by a fast secondary neutron, which in turn interacts, emits a fast proton interacting again and generating a π^0 and a neutron which interacts further downstream near the end of the visible volume.

this part of the elasticity distribution induce uncertainties of about 10 cm. The strongest test regarded the cascade length, because its energy dependence (fig. 7) had the strongest impact on the size of the neutron background. The measurements confirmed the predicted cascade length.

In conclusion, the special run with protons in Gargamelle confirmed the neutron background calculation in all respects. An example of a cascade in Gargamelle induced by a 7 GeV incident proton is shown in fig. 9.

Much later another check [127] was possible in the bubble chamber BEBC, when it was equipped with an Internal Picket Fence. The additional time information allowed a direct measurement of the neutron background and was found in good agreement with the one predicted by the neutron background program (sect. **2**˙1.1).

2˙4. *One year after the discovery.* – A year later the confusion got cleared up and an unambiguous picture emerged. The Gargamelle Collaboration withstood all criticism and was now confirmed by a considerable amount of evidence for weak neutral currents.

– Gargamelle:
Statistics doubled in agreement with first analysis [19]; furthermore corroboration of the background estimate by the Internal method [22]

– Single π production [23]:
In the 12 foot bubble chamber with hydrogen and deuterium filling at the Argonne National Laboratory a significant number of events in the processes $\nu p \to \mu^- p\pi^+$ and $\nu n \to \mu^- p\pi^0$ have been detected. This was the first observation of weak neutral currents in an exclusive channel.

– The CalTech FNAL Experiment:
A new counter experiment in the dichromatic Fermilab neutrino beam presented evidence of muonless events at the XVII International conference at London in July 1974 [24]; a new method based on the event length has been applied to distinguish efficiently events with muon from those without muon (see fig. 33).

– HPWF:
After all, the HPW collaboration understood their problem and now also observed muonless events [25].

The physics community was finally convinced of the existence of muonless events as claimed by Gargamelle. The systematic investigation of the new effect could start.

3. – The electroweak theory

3˙1. *The genesis: The Glashow-Salam-Weinberg model (GSW).* – At the beginning of the 1960s the experimental investigation of weak interactions entered a new phase with the advent of proton synchrotrons at CERN in Europe and BNL, ANL and NAL in the United States. Neutrino beams, the tool *par excellence* to study weak interactions, were built and opened the multi-GeV regime.

The success of the $V - A$ theory could not hide the serious deficiency, that it had no predictive power. The source of the problem was the bad high-energy behaviour. The total neutrino-nucleon cross section, for instance, was increasing linearly with energy. The massive intermediate vector boson (W), though not yet known to exist, would produce a damping through the propagator effect, yet the cross section of $(\nu\overline{\nu})$-scattering would still diverge. Novel processes had to be invoked in order to get the high energy behaviour under control. The result of the concerted effort of many theoreticians was a renormalizable model describing weak and electromagnetic interactions. An account of the making of this model is given by Veltman [27] and Weinberg [28]. It was first formulated for leptons. The naive extention to quarks led to a problem: the neutral current involving the Cabibbo current necessarily implied the occurrence of flavour-changing neutral currents, which however were known from strange-particle decays to be strongly suppressed. Glashow, Iliopoulos and Maiani [30] proposed a new current orthogonal to the Cabibbo current introducing a new u-type quark, the *charmed* quark, which was observed 4 years later. In this way the unwanted strangeness-changing neutral currents

were compensated and thus the problem cured. The fundamental work of Veltman and 't Hooft [31, 32] has proven the renormalizability of the model.

The physicists of the Gargamelle group were attracted by the model only after the proof of its renormalizability was brought to their attention. Then the question of whether or not the claimed weak neutral currents existed changed the priorities of the experiment which was already running since more than a year. Once the weak neutral currents were discovered by Gargamelle, models to explain the new type of events proliferated. The Glashow-Salam-Weinberg model was just one out of a host of others. However, within only about five years almost all alternatives to GSW could be ruled out and the time has come to call it the *Standard Model*.

3˙2. *The final form.* – The electroweak theory is since long treated in textbooks and monographs, for instance [26, 29, 35, 39-42]. It is not the intention to compete with them, but rather to highlight some of the salient features and relate them to their experimental verification.

The electroweak theory is based on the local $SU(2) \times U(1)$ gauge group. It is spontaneously broken down to $U(1)_{\mathrm{em}}$. This implies that the longstanding QED is no longer a theory by itself, but part of the larger gauge group, and has therefore a limited region of validity (c.f. [26] p. 93). Its predictions remain valid as long as the relevant invariants are small compared to the weak boson masses, otherwise the full theory must be taken into account.

Three sectors can be distinguished:

– Gauge boson sector: the spin-1 particles $W^{\pm}$, Z, γ.

– Fermion sector: 3 families of spin-(1/2) particles.

– Higgs sector: the spin-0 Higgs-particle.

The theory contains a large number of free parameters, which are related to the couplings, the particle masses and the mixing:

– Couplings: 4 effective charge form factors (fig. 10).

– Masses:
  a) Gauge bosons: M_W, M_Z and the massless γ.
  b) Fermion masses: 6 quark masses and 6 lepton masses.
  c) Higgs mass: M_H.

– Mixing parameters: 2 unitary matrices of the quark and the lepton sectors.

The electroweak theory is a renormalizable gauge theory. This means that any electroweak quantity can be predicted in terms of a finite number of parameters. These parameters must be obtained from experiment. Once a complete set of defining relations has been established, any further quantity can be predicted to an accuracy limited by the numerical precision of the free parameters. During the first years after the discovery of weak neutral currents the only precisely known quantities were the Fermi coupling constant G_μ and the fine-structure constant α. The mixing of electromagnetic and weak phenomena is expressed by the new parameter $\sin^2\theta_w$, where θ_w is the *weak mixing angle*. Its initial measurement in neutrino experiments served to make predictions for quantities at Born level. A prominent example was the prediction of the mass of the W

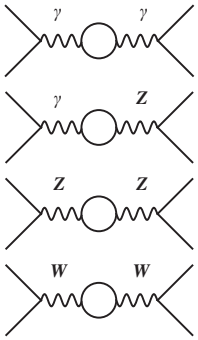

Fig. 10. – The graphs corresponding to the $\gamma\gamma$, γZ, ZZ and WW propagator degrees of freedom.

1976 using the relation $M_W = 37\,\mathrm{GeV}/\sin\theta_w$, where the energy scale is determined by the ratio G_μ/α of the couplings responsible for weak and electromagnetic interactions.

As soon as precise predictions are required the full theory comes into play. The 1-loop corrections involve the full set of input parameters.

Such a set of input parameters is called a *renormalization scheme*. The *on shell scheme* consists in the choice α, M_W, M_Z, m_f or G_μ, M_W, M_Z, m_f. They are not independent. The following relation holds:

$$G_\mu = \frac{\pi\alpha}{\sqrt{2}M_W^2 \sin^2\theta_w}\frac{1}{1-\Delta r}\,, \tag{3}$$

where Δr accounts for radiative effects, depending on α and all masses of the Standard Model including the Higgs mass. The electroweak parameter $\sin^2\theta_w$ requires a careful definition.

– In the on-shell scheme the definition of $\sin^2\theta_w$ is given by the ratio of the gauge boson masses: $s_W^2 = 1 - \frac{M_W^2}{M_Z^2}$. According to the above formula all terms are well known except for Δr, which has to be evaluated in perturbation theory. It is found [132] that $\Delta r \sim \Delta r_0 - \frac{\rho_t}{\tan^2\theta_W}$ and $\Delta r_0 = 1 - \frac{\alpha}{\hat{\alpha}(M_Z)} = 0.06635 \pm 0.00010$ takes into account the running of α and $\rho_t = \frac{3G_\mu m_t^2}{8\sqrt{2}\pi^2} = 0.00943\,(m_t/173.4\,\mathrm{GeV})^2$ represents the main (quadratic) m_t dependence.

– A more refined quantity is $s^2_{M_Z}$ defined by: $s^2_{M_Z}(1-s^2_{M_Z}) = \frac{\pi\alpha(M_Z)}{\sqrt{2}G_F M_Z^2}$. It depends on M_Z which is much better known than M_W. The (m_t, M_H) dependence is removed from Δr and $(\alpha(M_Z))^{-1} = 128.93 \pm 0.02$.

– The LEP groups have used $\sin^2\theta^{\mathrm{lept}}_{\mathrm{eff}} = \frac{1}{4}(1 - \frac{v_e}{a_e})$ defined at the Z-pole.

– In the modified minimal subtraction scheme ($\overline{MS}$) $\sin^2\theta_w$ is defined by the $SU(2)\times U(1)$ gauge couplings g and g'. The quantity $\hat{s}^2_Z(\mu) = \sin^2\hat{\theta}_w(\mu) = \frac{\hat{g}'^2(\mu)}{\hat{g}^2(\mu)+\hat{g}'^2(\mu)}$ is introduced, where $\hat{g}$ and $\hat{g}'$ are renormalized in the modified minimal subtraction scheme and depend on the scale μ. The scale can be chosen conveniently. For the confrontation of theory with the low-energy neutrino data $\mu = 0$ is convenient, whereas for the LEP/SLD data $\mu = M_Z$. In ref. [43] a more refined quantity $\overline{s}^2(\mu)$

is introduced, which differs from $\hat{s}^2(\mu)$ by a so-called pinch term. The μ-dependence allows to check the running of the charge form factors from $q^2 = 0$ to $q^2 = M_Z^2$.

– The sensitivity to new physics depends on which definition of $\sin^2\theta_w$ is used.

– Relations:
The different definitions above are related to each other: $\hat{s}_Z^2 = c(m_t, M_H)s_W^2 = \overline{c}(m_t, M_H)s_{M_Z}^2$; $c = 1.0362 \pm 0.0004 \sim 1 + \rho_t/\tan^2\theta_w$ and $\overline{c} = 1.0009 \mp 0.0002 \sim (1 - \rho_t/(1 - \tan^2\theta_w))$. $\sin^2\theta_{\rm eff}^{\rm lept} = \overline{s}^2(M_Z^2) + 0.0010$.

Weak neutral current processes such as $\nu e \to \nu e$, $\nu q \to \nu q$, $e^+e^- \to l^+l^-$ $(l = e, \mu, \tau)$ belong to the generic class of 4-fermion interactions $ff' \to ff'$ described by the matrix element [43]

$$T_{ff'} = C_{ff'} J_f J_{f'}. \tag{4}$$

It involves the currents $J_f^\lambda = \overline{\psi}_f \gamma^\lambda (1 \pm \gamma_5)\psi_f$ and similarly for f'. Any fermion field can be decomposed into a left-handed and right-handed part

$$\psi = \psi_L + \psi_R = \frac{1}{2}(1 + \gamma_5)\psi + \frac{1}{2}(1 - \gamma_5)\psi,$$

since the projection operators $1 \pm \gamma_5$ are orthogonal. This allows to put the left- and right-handed components of the fermions into independent representations under $SU(2)$, namely left-handed doublets L_f (lepton and quark sectors) and right-handed singlets R_f,

$$L_l = \frac{1}{2}(1 + \gamma_5)\begin{pmatrix}\nu_l \\ l\end{pmatrix}, \qquad L_q = \frac{1}{2}(1 + \gamma_5)\begin{pmatrix}q \\ q'\end{pmatrix}, \qquad R_f = \frac{1}{2}(1 - \gamma_5)f,$$

with $l = e, \mu, \tau$ and $q = u, c, t$ and $q' = d, s, b$. The amplitude $C_{ff'}$ in 1-loop is given in ref. [43] and displayed in eq. (5) dropping vertex and box contributions. It depends upon the charge form factors $\overline{e}^2(s)$ and $\overline{g}_Z^2(s)$ (see fig. 10), the electromagnetic and weak charges and the propagators.

$$C_{ff'} = \overline{e}^2(s)\frac{Q_f Q_{f'}}{s} + \overline{g}_Z^2(s)\frac{Q_f^w Q_{f'}^w}{s - M_Z^2 + i\Gamma_Z M_Z}\,, \tag{5}$$

$\overline{e}^2(0)$ is fixed by the fine-structure constant α, *i.e.* $\overline{e}^2(0) = 4\pi\alpha$. The weak charges are $Q_f^w = I_3 - Q_f\,\hat{s}^2$ with the weak isospin component I_3 being $\pm 1/2$ or 0 and the electromagnetic charge Q_f of the fermion f.

Radiative effects consist of bremsstrahlung, vertex, box and propagator corrections. Bremsstrahlung can be treated separately. Vertex and box corrections are process-dependent, while the propagator corrections (see fig. 10) are universal. A complete elaboration is given in ref. [43]. There the propagator corrections are characterized by the four effective charge form factors: $\overline{e}^2(q^2)$, $\overline{s}^2(q^2)$, $\overline{g}_Z^2(q^2)$, $\overline{g}_W^2(q^2)$. They evolve with the relevant 4-momentum transfer squared and prove useful even at $|q^2| \gg M_Z^2$. Their determination is explicitly given at the two scales q^2=0 and M_Z^2 including all experimental data up to 1997. Figure 13 shows all low-energy neutral-current experiments in the plane given by the two charge form factors $\overline{s}^2$ and $\overline{g}_Z^2$. In the (minimal) Standard Model each of the charge form factors can be predicted in terme of $m_{\rm top}$ and $M_{\rm Higgs}$.

The low-energy form of the electroweak theory reproduces the $V - A$ theory and QED. It is *a posteriori* understood, in which sense these two theories had similarities despite the substantial differences. For a long time the communities investigating weak and electromagnetic phenomena operated independently. Only with the advent of weak neutral currents a definite incentive was given to search for an interference between the known electromagnetic neutral current and the new weak neutral current (see sect. **4**˙3).

3˙3. *The crucial experimental tests.* – With 't Hooft's proof of renormalizability [31] (1971) the GSW model supplemented with the GIM mechanism held the promise of a breakthrough in understanding electromagnetic and weak interactions. At that moment, however, none of the theoretical ingredients had experimental support: there was no evidence for weak neutral currents, no evidence for the carriers of the weak forces, no evidence of the Higgs boson responsible for the mass generating mechanism, and no evidence for the GIM mechanism. Once the weak neutral currents were discovered the major steps of the future research could be anticipated. The achievements along this line represent a true success story of the interplay between experiment and theory.

3˙3.1. Testing the Born level. At lowest order the electroweak theory is very simple, as its predictions depend on a single parameter $\sin^2\theta_w$, where θ_w is the mixing angle. Experiments during the decade 1973-1983 focussed on measuring this parameter in various reactions and showing numerical agreement (many neutrino experiments, the SLAC-Yale experiment [57], atomic parity violation). Right from the beginning importance was attached to model-independent determinations of the weak couplings $Z \to f\overline{f}$. This was forcefully pushed by Sakurai. It should be noted that the GSW model was in competition with numerous other models. For that reason model-independent parameters served to eliminate efficiently competing models claiming also weak neutral currents.

3˙3.2. The multiplet structure. The fermions are classified as left-handed isodublets and right-handed singlets and occur in three families. Shortly after the discovery of weak neutral currents states with the new quantum number *charm* were observed. It now became obvious that the leptons and quarks form a family structure consisting of doublets $(ud)(\nu_e e)$ and $(cs)(\nu_\mu \mu)$. The immediately following observations of the heavy lepton τ and the heavy quark b suggested a third family $(tb)(\nu_\tau \tau)$ and led to the postulation of a new neutrino as partner of the τ lepton (called ν_τ) and a heavy *up*-type quark as partner of the b-quark (called t) [36,37]. Once the free parameters of the theory were sufficiently precise, it was possible to predict the mass of the top quark through its dependence in the 1-loop corrections. Later, 1995, it was observed at the Tevatron at the predicted mass. Meanwhile, the mass is measured to a precision of 1 GeV. The neutrino of the third family was observed 2001 by the DONUT Collaboration [53].

3˙3.3. The gauge bosons. After about 5 years GSW remained as the only serious candidate for a theory of electroweak interactions. It described consistently all low energy data with $\sin^2\theta_w = 0.23$ measured to 10%. The next major step consisted in finding the weak gauge bosons, the carriers of the weak interactions. It was in this period that the term *electroweak* was coined. The masses of the gauge bosons are proportional to the vacuum expectation value, which in turn is related to the Fermi coupling constant. The early measurements of $\sin^2\theta_w$ allowed to predict the masses of the weak bosons with the result that they were far beyond reach with the existing techniques. The frontier in energy had to be pushed up. The new facility $S\overline{p}pS$ at CERN colliding protons and

antiprotons allowed to generate $W^{\pm}$ and Z exactly 10 years after the discovery of weak neutral currents [38].

3˙3.4. 1-loop level. The full theory brings in all electroweak parameters. Predictions depend upon the numerical values of all masses (including the masses of the top quark and the Higgs boson) and couplings. At the beginning of the e^+e^- collider experiments at DESY, SLAC and KEK it was difficult to compare data, because each group evaluated the radiative effects with different sets of input paramters. This drawback could only be overcome by experiments with increased precision and by new machines of higher energy. This challenge was met by the collaborations working at LEP, SLC, Tevatron.

3˙3.5. The non-Abelian character. The fact that the electroweak theory is based on a non-Abelian group entails that the weak gauge bosons interact with each other. The theory contains triple-boson vertices of the form WWZ and $WW\gamma$. Their existence has been demonstrated at LEP II [37].

3˙3.6. The Higgs sector. The crowning step consists in establishing the Higgs particle, the scalar boson responsible for giving mass to the fermions and the gauge bosons. The standard electroweak theory fixes all properties of that unique particle except for its mass. LEP II has set a lower limit of 114 GeV. The analyses at the Tevatron with ever increasing luminosity have reduced the available phase space to small mass windows. On July 4, 2012 the two LHC Collaborations ATLAS and CMS have announced the observation of a resonance at 125 GeV at a significance level of 5 standard deviations. Each collaboration has analysed and combined their data of 2011 at 7 TeV and 2012 at 8 TeV corresponding to a luminosity of about $10\,\mathrm{fb}^{-1}$. The production rate of the new particle and the branching ratios in $\gamma\gamma$ and 4 leptons are consistent with the properties of the Higgs boson.

4. – The experiments

4˙1. *Overview.*

4˙1.1. The rise to the Standard Model. A rapid series of experiments has filtered out of the host of models proposed to explain the phenomenology of weak neutral currents essentially one: the Glashow-Salam-Weinberg Model. The prediction of the Born processes depended only upon a single parameter, the *weak angle* θ_w, and made the comparison with the measurements easy and straightforward. It came as a surprise that an algebraic structure as simple as $SU(2) \times U(1)$ would describe so successfully the data.

The first years after the discovery were dominated by neutrino experiments with bubble chambers (Gargamelle at CERN, the 15′ bubble chamber at FNAL, the 12′ at Argonne, the 7′ at Brookhaven, SKAT at Serpuchov) and the electronic detectors (HPWF and CITF at FNAL). The measured quantity was mainly the ratio NC/CC of the inclusive weak neutral- and charged-current processes with a typical precision of 10–20%.

In a second series of ν and $\overline{\nu}$ experiments Gargamelle was operated with the light liquid propane C_3H_8 with the aim to study also exclusive processes, *i.e.* single-pion production both for neutral and charged currents. A remarkable feature was that now interactions also on free protons could be investigated. Figure 11 shows the excitation of the $\Delta(1236)$ resonance observed for the first time by the weak neutral current [114]. The very fact of observing the transition $p \to \Delta^{++}$ eliminated models without isospin change, *i.e.* $\Delta I = 0$. The single pion data provided useful tests of isospin structure of the

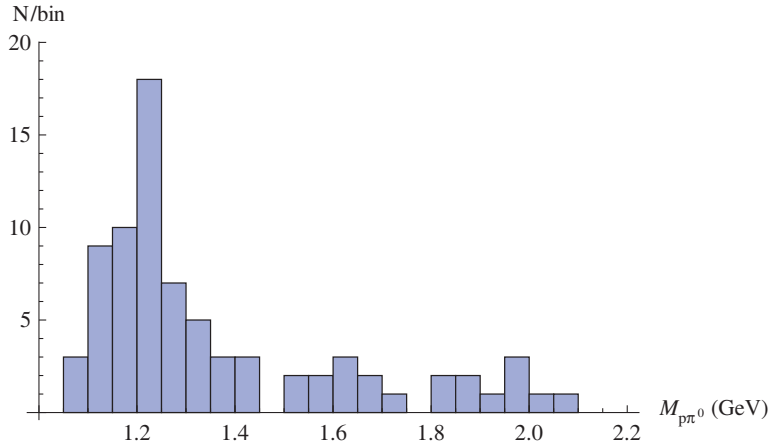

Fig. 11. – Excitation of the 1236-resonance by the weak neutral current.

weak neutral and charged currents. It demonstrated the capability of bubble chambers that even the process $\nu + n \to \nu + n + \pi^0$ could be measured, although all particles in the final state were neutral, thus without generating tracks at the interaction point in the chamber. The single pion data played again, 20 years later, a role in interpreting the Kamioka experiments.

With the commissioning of the SPS accelerator, three years after the discovery, a new and fruitful period started at CERN. Together with Gargamelle three new detectors came into operation: the bubble chamber BEBC and the two calorimeters of the CDHS and the CHARM collaborations. It was now possible to investigate neutrino interactions in the energy regime from 10 to a few hundred GeV with intense wide and narrow band beams. At Fermi lab two new collaborations, CCFR and FMMF, started data taking. Neutrino physics was no longer a field of low statistics. Even bubble chambers could now register one event per picture.

The (γ, Z) interference was investigated in two types of experiments by measuring parity violation in heavy atoms, starting with bismuth, and at SLAC in polarized electron deuteron scattering [57]. The required sensitivities were 10^{-7} and 10^{-4}, respectively. The *ed* experiment yielded a clear signal and established in this way an essential property of the weak neutral current. The analogon of this experiment in the neutrino sector was the measurement of the single π^0 channel induced by a neutrino (left-hander) and an antineutrino (right-hander). The final hadron state was equal in both cases. The difference of the cross sections turned out to be significantly different from 0. However, the first measurements on atoms resulted in no effect contrary to the expectation of the GSW model. Only after many years of experience also the measurements on atoms got precise results.

Apart from the technically difficult experiments on atoms a consistent picture emerged with a common value of $\sin^2\theta_w$ already from all measurements within the first five years and was gradually consolidated (cf. fig. 12 [13], fig. 13 [43, 44]). This was taken as convincing case in favour of the GSW Model (Nobel prices for Glashow, Salam and Weinberg in 1979). Since then the GSW Model served as standard reference for the interpretation of any new measurement and thus became the *Standard Model*.

So far the Born processes were considered. The main task was now to find out whether the GSW model is really a gauge theory based on the spontaneously broken non-Abelian

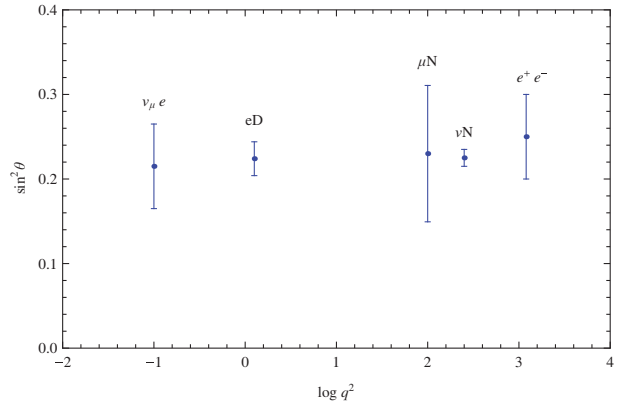

Fig. 12. – Values of $\sin^2\theta_w$ from various areas in 1984.

algebra $SU(2) \times U(1)$. A systematic investigation of all three sectors of the theory set in, namely the gauge boson sector (spin 1), the fermion sector (spin 1/2) and the Higgs sector (Spin 0).

4˙1.2. Precision neutrino experiments. A workshop was held in 1981 [58] to discuss the possibility of measuring radiative effects in neutrino scattering experiments. If the measured cross section ratio NC/CC is interpreted in terms of $\sin^2\theta_w$ using once the Born approximation and once the full cross sections including 1-loop corrections, the resulting value of $\sin^2\theta_w$ gets shifted by 0.01. The challenge was then to increase the precision in measuring NC/CC to ± 0.005. The collaborations CDHS and CHARM took up the challenge and eventually succeeded (see [26] and sect. **4**˙3). This was an important step

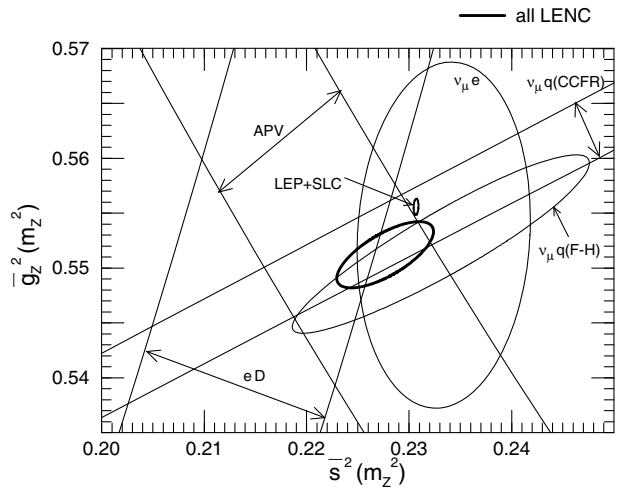

Fig. 13. – Fit of all low-energy neutral-current experiments as of 1997 in terms of $\bar{s}^2(M_Z^2)$ and $\bar{g}_Z^2(M_Z^2)$ calculated from $\bar{s}^2(0)$ and $\bar{g}_Z^2(0)$ assuming Standard Model running in order to compare with Z-pole data. The thick ellipse is the $1-\sigma$ contour of the combined fit.

in testing the electroweak theory. During this period neutrino physics reached precision status. BEBC was now equipped with an *external muon identifier (EMI)* and with an *internal picket fence (IPF)*. This ensured a better distinction of NC and CC events and a better rejection of the neutron background. It was possible to disentangle the couplings $Zu\overline{u}$ and $Zd\overline{d}$.

4˙1.3. e^+e^- colliders. The low-energy e^+e^- colliders were the classic tools to study electromagnetic phenomena. With PETRA and PEP coming into operation in 1978 for the first time machines with high enough energy were available to detect deviations from pure QED. The model of electroweak interactions predicted small interference effects between the electromagnetic and weak amplitudes (see eq. (6)) implying, for instance, a small angular asymmetry in the purely leptonic process $e^+e^- \to l^+l^-$. In practice the muon channel was first used to make a clean test. Indeed, three years after the commissioning of PETRA the four collaborations JADE, MARKJ, PLUTO (later also CELLO), TASSO had combined their first event samples of $e^+e^- \to \mu^+\mu^-$ and could report to the Lepton-Photon Conference in 1981 at Bonn an asymmetry in the angular distribution, thus a clear sign of a deviation from QED. The observed pattern of deviation consisted of an additional contribution proportional to $\cos\theta$ and confirmed the prediction by GSW, infact the first test in the time-like region. With increasing statistics the distributions of fig. 14 were obtained [46]. To be more specific the interference occurs between the electromagnic vector current and the weak axial-vector current and thus not parity violating. It provided a measurement of the axial-vector coupling constant a_μ.

The differential cross section of $e^+e^- \to l^+l^-$ $(l = e, \mu, \tau)$ is given by

$$\frac{\mathrm{d}\,\sigma}{\mathrm{d}\,\cos\theta} = \frac{\pi\alpha^2}{2s} R_l \left(1 + \cos^2\theta + \frac{8}{3} A_l\, \cos\theta\right), \tag{6}$$

where A_l is the angular asymmetry and R_l is the total cross section in terms of the point-like QED cross section $\sigma_0 = 4\pi\alpha^2/3s$. The electroweak theory predicts both quantities

$$R_l = Q_e^2 Q_l^2 + 2v_e v_l Q_e Q_l Re\chi + (v_e^2 + a_e^2)(v_l^2 + a_l^2)|\chi|^2, \tag{7}$$

$$A_l = \frac{1}{R_l} Q_e Q_l \left(\frac{3}{2} a_e a_l Re\chi + 3 v_e v_l a_e a_l |\chi|^2\right), \tag{8}$$

$$\chi = \frac{\sqrt{2} G_\mu M_Z^2}{4\pi\alpha} \frac{s}{s - M_Z^2 + i M_z \Gamma_z}\,. \tag{9}$$

The propagators of the γ and Z generate the characteristic energy dependence: the $1/s$ falloff at small energy followed by the resonance behaviour around the Z-mass. This is seen in fig. 15, where the data of several e^+e^- colliders were put together [52]. The measurement of R_l is rather insensitive to the vector coupling constant at PETRA/PEP energies, since $v_l = -\frac{1}{2} + 2\sin^2\theta_w \approx 0$.

The PETRA energy was continuously increased with the aim to find the top quark, the presumed isodublet partner of the b-quark discovered in 1977. Simple conjectures suggested masses of the top quark around 18 GeV or slightly above, but neither a resonance analogous to the Υ nor an increase in the total hadronic cross section was observed and after reaching the limiting PETRA energy one had to conclude that the top quark, if it exists, has a mass larger than 23 GeV.

When PETRA terminated operation in 1986, TRISTAN (1986-1995) at KEK took over and extended the investigations up to center-of-mass energies of 64 GeV with three

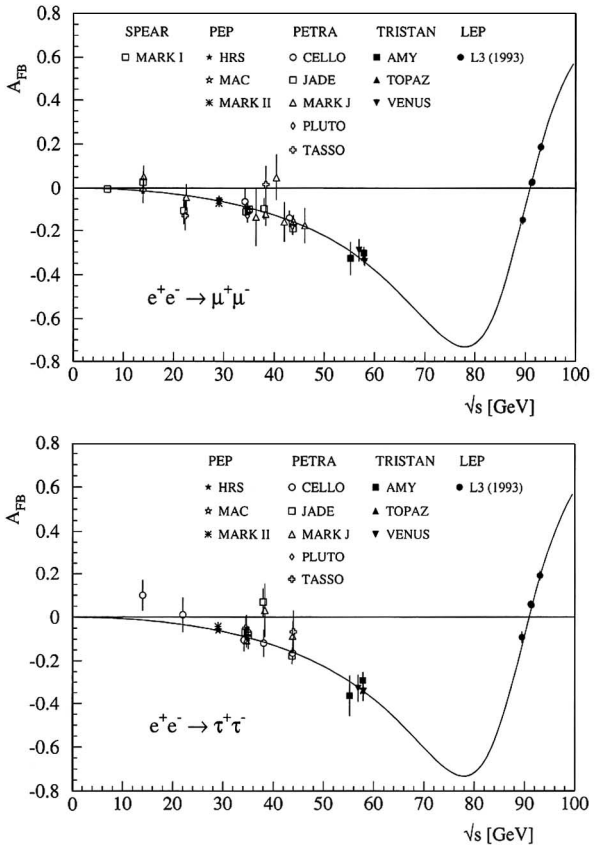

Fig. 14. – Angular asymmetries in $e^+e^- \to \mu^+\mu^-$ and $\tau^+\tau^-$.

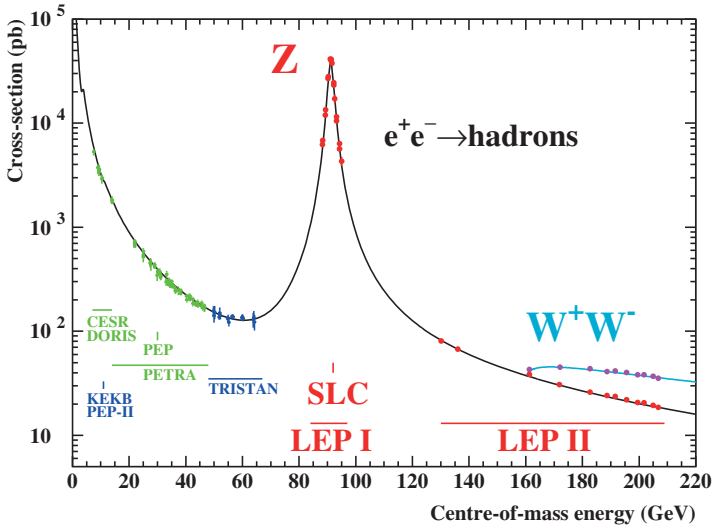

Fig. 15. – The total cros section of $e^+e^- \to$ *hadrons* as a function of the collider energy. The solid line is the prediction of the Standard Model.

omnipurpose detectors AMY, TOPAZ and VENUS. The hope to discover the top quark was not fulfilled. The destructively interfering electromagnetic and the weak amplitudes were now of similar size and led to small cross sections, but large asymmetries, particularly for the heavy flavours.

While TRISTAN was still running the SLC and LEP e^+e^- colliders started in 1993 operation at and around the Z-resonance. The MARKII, SLD detectors at SLAC and the 4 large detectors ALEPH, DELPHI, L3 and OPAL at LEP investigated the properties of the Z and the weak neutral current with unprecedented precision.

The increasingly stringent tests of the Standard Model [117] moved the question of what the origin of the electroweak symmetry breaking is more and more into focus. The machine energy of LEP was gradually upgraded until slightly above 110 GeV, but no indication of the SM Higgs boson was found. The energy was big enough to study W^+W^- production and the triple boson vertex (see for instance fig. 11 in ref. [37]). LEP II was switched off in 2001 to give way to the LHC.

4˙1.4. The weak bosons. With the discovery of weak neutral currents strong hope existed to find sooner or later the carriers of the weak forces, $W^\pm$ and Z, as real particles. The signature for the W since the very first neutrino experiments was either their direct production and leptonic decay or a deviation of the total cross section from the linear rise in the neutrino energy. No evidence was found and the GSW model provided an explanation why that was so. The early measurement of $\sin^2\theta_w$ together with the theoretical relation between the masses of the weak bosons and the weak angle θ allowed to predict the numerical value for them and turned out to be way out of reach for neutrino experiments. It was the proposal of Cline, Mc Intyre and Rubbia at the Aachen Neutrino Conference 1976 to build a $p\overline{p}$ collider in order to reach the required center of mass energy. Their idea was realized at CERN. The two experiments of the UA1 and UA2 collaborations observed in 1983 for the first time both the W and the Z bosons. This was a great achievement.

In the coming years a forceful program was accomplished at CERN with UA1, UA2 and at FNAL with CDF,D0. Precise measurements were obtained for the masses of W and Z. The searches for the Higgs led to excluded regions leaving finally, when the Tevatrons was shut down, only a small interval around 125 GeV. It was the great highlight on July 4, 2012 when ATLAS and CMS presented the discovery of a resonance consistent with the long searched for Higgs particle.

4˙1.5. The ep collider HERA. The deep inelastic scattering using electron or muon beams was for a long time a domain of QED and therefore, since QED was well understood, served to investigate strong interactions, in particular the study of the DGLAP (Dokshitzer, Gribov, Lipatov, Altarelli, Parisi) evolution equations. Nearly two decades later, at the beginning 1990s, the electron-proton collider HERA with the center-of-mass energy of 300 GeV came into operation. Its energy is so large, that weak and electromagnetic processes could be studied simultaneously. Figure 16 illustrates this. At low momentum transfer neutral-current processes are dominated by QED and are by two orders of magnitude stronger than weak-charged-current processes. This was the situation in the 1970s and makes clear in retrospect why the communities using charged lepton beams and neutrino beams were working quite independently of each other. The large gap in cross section reflects the propagator effect of the photon and the Z. Despite the smallness of the weak current admixture, the ed experiments 1977 at SLAC succeeded in proving the $\gamma - Z$ interference for the first time and in demonstrating parity violation of

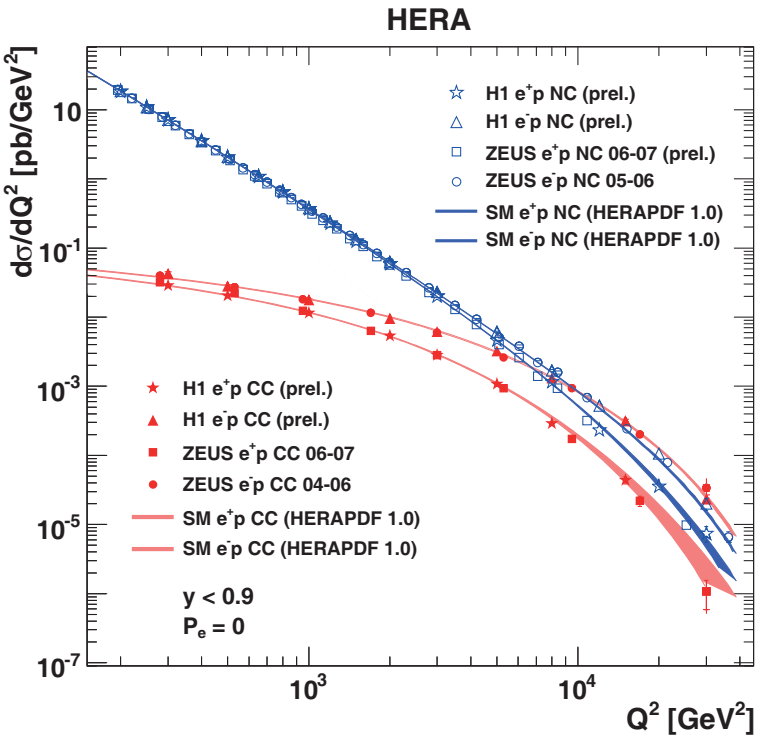

Fig. 16. – NC and CC cross sections *vs.* Q^2 at HERA.

the weak neutral current. Once the momentum transfer increases up to the weak boson masses the amplitudes of the electromagnetic and the weak currents become of similar order. Thanks to the large center-of-mass energy of HERA the process $ep \to \nu_e + anything$ could be observed for the first time. It is the inverse of neutrino scattering and corresponds, if interpreted as fixed target experiment, to a beam energy of 30 TeV, large enough to exhibit the effect of the W-propagator in the total cross section.

4˙2. *Purely leptonic interactions.*

4˙2.1. Introduction. There are four neutrino-electron scattering processes:

1) $\overline{\nu_\mu} e^- \to \overline{\nu_\mu} e^-$,

2) $\nu_\mu e^- \to \nu_\mu e^-$,

3) $\nu_e e^- \to \nu_e e^-$,

4) $\overline{\nu_e} e^- \to \overline{\nu_e} e^-$.

The processes 1) and 2) occur only via the weak neutral current, while processes 3) and 4) receive also contributions from the weak charged current. The relevant lower-order Feynman diagrams are illustrated in fig. 17. Their cross sections are proportional to the square of the total center-of-mass energy $s = (2m_e E_\nu) + m_e^2$ and are therefore very small,

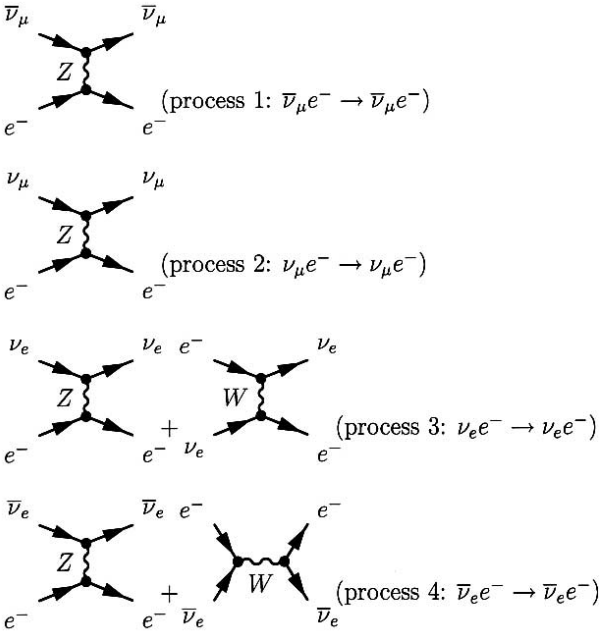

Fig. 17. – Lower-order Feynman diagrams for purely leptonic ν and $\overline{\nu}$ scattering off electrons.

namely on the order of $10^{-42}\,\mathrm{cm}^2\,E_\nu/\mathrm{GeV}$. The angle between the emitted electron and the direction of the incoming ν is very small

$$\theta \leq \sqrt{\frac{2m_e}{E_e}}\,.$$

Hence the general requirements on detectors for measuring such reactions are

– large mass to be sensitive to very small cross sections,

– excellent angular and energy resolutions to discriminate against ν-induced background, *e.g.* $\nu_e + n \to e^- + p$ (*invisible*).

In addition to the purely leptonic weak neutral-current-induced processes there are also those involving both weak and electromagnetic neutral currents, *e.g.*

5) $e^+e^- \to e^+e^-$,

6) $e^+e^- \to l^+l^-$,

7) $e^-e^- \to e^-e^-$,

with the lower-order Feynman diagrams shown in figs. 23, 24, 25. The total cross section for these processes consists of the following terms:

a) e.m. term,

b) weak term (leptonic N.C.),

c) interference term,

which imply the characteristic energy dependence displayed in fig. 15. At low energies ($Q^2 \ll M_Z^2$), where the electromagnetic term dominates, only the interference term can be experimentally observed, while at $Q^2 \simeq M_Z^2$ the weak term is dominating (cf. sect. **4**˙1.3).

This section covers the experiments with neutrinos scattering off electron, followed by Moeller scattering and lepton pair production $e^+ + e^- \to l^+ + l^-$ at PETRA and PEP (interference term) and concludes with the experiments at the Z-resonance performed at CERN and SLAC.

4˙2.2. Discovery of the purely leptonic neutral current: 1973. The very first example of the reaction 1) was observed by the Aachen group of the Gargamelle Collaboration and interpreted as manifestation of weak neutral currents. The celebrated event is shown in fig. 18. A total of 360000 pictures was scanned twice by the Collaboration [10]. The event occurring in the $\overline{\nu}$ film consists of just an isolated track in beam direction. Its unambiguous identification as electron is based on the curvature of the track, the spiralization and the bremsstrahlung. The electron energy was 385 ± 100 MeV and the angle to the $\overline{\nu}$ beam axis was $1.4^{+1.6}_{-1.4}$ degrees. The main source of background was

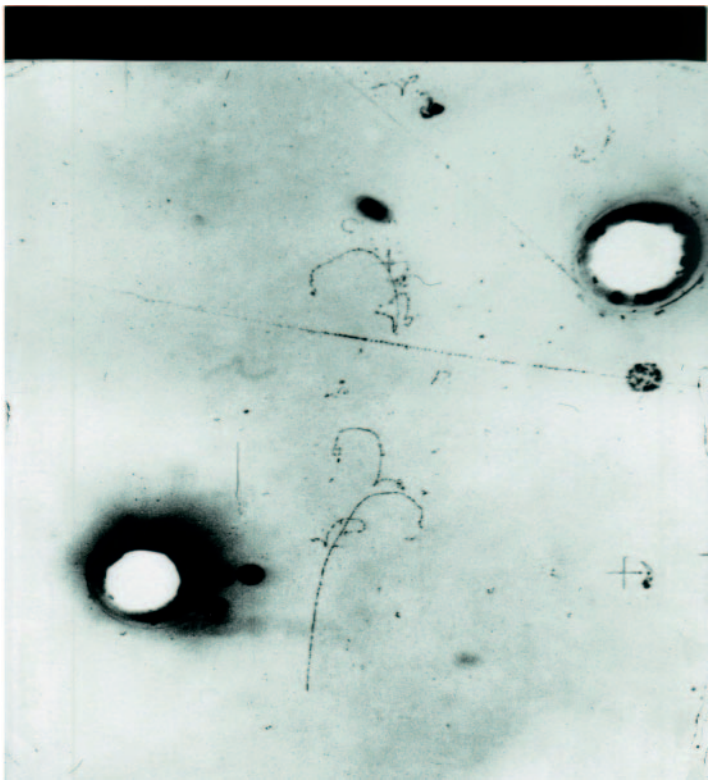

Fig. 18. – GGM discovery of reaction 1): $\overline{\nu}_\mu e \to \overline{\nu}_\mu e$.

due to the small contamination of ν_e in the $\overline{\nu}_\mu$ beam. The process $\nu_e + n \to e^- + p$ can simulate the neutral-current configuration, if the electron is emitted in the forward direction (angle $< 5°$) and if the final-state proton remains unobservable. The total background is however small and was estimated to contribute 0.03 ± 0.02 events.

The final search for $\nu_\mu e^-$ and $\overline{\nu}_\mu e^-$ elastic scattering by the Gargamelle Collaboration refs. [83, 84] yielded the cross sections per electron in cm^2 as function of the energy in GeV at 90% confidence level

$$\sigma(\overline{\nu_\mu} + e^- \to \overline{\nu_\mu} + e^-) = (1.0^{+2.1}_{-0.9})\ 10^{-42}\ E_{\overline{\nu}}, \tag{10}$$

$$\sigma(\nu_\mu + e^- \to \nu_\mu + e^-) \leq 3\ 10^{-42} E_\nu. \tag{11}$$

It was then possible to quote, for the first time, the range $0.1 < \sin^2\theta_w < 0.6$ for the weak angle in the Glashow-Salam-Weinberg Model.

4˙2.3. Confirmations in the seventies. After the discovery many experiments confirmed the Gargamelle results, as reported in table IV.

TABLE IV. – *Experiments in the seventies.*

Reaction	Experience/Ref.	Energy	N (ev)	Background	$\sin^2\theta_w$
$\overline{\nu}_e + e^- \to \overline{\nu}_e + e^-$	Reines (1976) [77] Plastic scint. (16 kg)	$(1.5 - 3)$ Mev	5.9 ± 1.4	$\leq 0.13\%$	0.29 ± 0.05
$\overline{\nu}_\mu + e^- \to \overline{\nu}_\mu + e^-$	Gargamelle PS 1976 [83]	0.3-2 Gev	3.	0.44 ± 0.13	0.25 ± 0.15
$\overline{\nu}_\mu + e^- \to \overline{\nu}_\mu + e^-$	Aachen-Pd(19 tons) Sp.Ch. [85]	0.3-2 Gev	7.	2.0 ± 0.3	0.38 ± 0.07
$\nu_\mu + e^- \to \nu_\mu + e^-$	Aachen-Pd [86]	(0.2-2) GeV	11	5.4 ± 0.5	0.38 ± 0.07
$\nu_\mu + e^- \to \nu_\mu + e^-$	FNAL H_2 B.C. (1978) [88]	$\geq 2.$ GeV	11	0.8	$0.2^{+0.16}_{-0.08}$
$\nu_\mu + e^- \to \nu_\mu + e^-$	GGM-SPS(1979) (SPS) [89]	$\geq 2.$ GeV	9.8 ± 3.4	0.5 ± 0.3	$0.12^{+0.11}_{-0.07}$

4˙2.4. Experiments with higher statistics in the eighties. Enormous progress was achieved, as shown in table V.

In comparison with the earlier experiments in table IV the increased statistics allowed also the measurement of the differential distribution $\mathrm{d}\sigma/\mathrm{d}y$. The data were evaluated in terms of $\sin^2\theta_w$ and the vector and axial-vector couplings g_V and g_A. It is remarkable to note the high precision achieved despite the very low cross sections. The experiments in Brookhaven were realized using a Liquid Scintillator Calorimeter viewed by photomultiplier tubes and by a system of proportional drift tubes (total mass = 170 tons); the proton beam of the Alternating Gradient Synchrotron of BNL (28.3 GeV) impinged on a titanium target producing pions and kaons which in turn decayed into neutrinos

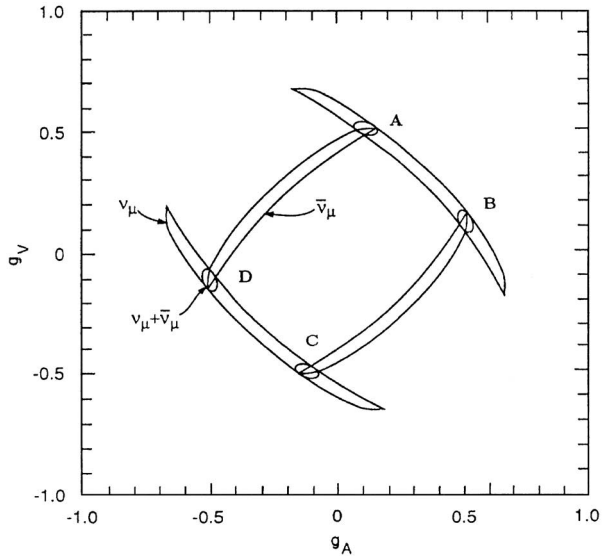

Fig. 19. – Results from the experiment E734: allowed bands in g_V and g_A plane due to the ν_μ and $\overline{\nu_\mu}$ data; their overlap define four solutions (A,B,C,D).

and antineutrinos for the experiment. The detector was able to measure the ν_μ spectra through the quasielastic interactions on nucleons. In fig. 19 are illustrated their results for the vector and axial-vector couplings with a fourfold ambiguity. Together with the results of other experiments the solution D was singled out.

CHARM-II was the experiment with the highest statistics in the late 1980s. They have exploited the ratio

$$R = \frac{\sigma(\nu_\mu e)}{\sigma(\overline{\nu}_\mu e)} = 3\frac{1 - 4\,\sin^2\theta_w + (16/3)\,\sin^4\theta_w}{1 - 4\,\sin^2\theta_w + 16\,\sin^4\theta_w}\,,$$

which is strongly dependent upon $\sin^2\theta_w$ and thus provides an accurate measurement of its value (see fig. 20). The CHARM-II detector consisted of a massive target calorimeter followed by a muon spectrometer. The calorimeter was instrumented with streamer tubes equipped with digital and analog readout to measure the energy and the direction

TABLE V. – *Experiments performed during the 80's. The last column quotes, where available, the vector coupling and below the value of* $\sin^2\theta_w$.

Reaction	Exp./Ref.	E/GeV	N (ev)	g_A	g_V ($\sin^2\theta_w$)
$\overline{\nu}_\mu + e^-$	E734(BNL)	1	$\simeq 98$	$-0.514 \pm 0.023 \pm 0.028$	-0.107 ± 0.035
$\nu_\mu + e^-$	refs. [92, 93]	1	$\simeq 160$		$0.195 \pm 0.018 \pm 0.013$
$\nu_\mu + e^-$	15 foot B.C. FNAL [94]	20	22		$0.20^{+0.06}_{-0.05}$
$\overline{\nu}_\mu + e^-$	CHARM II	23	$\simeq 2200$	-0.503 ± 0.018	0.025 ± 0.019
$\nu_\mu + e^-$	SPS [95]				$0.237 \pm 0.007 \pm 0.007$

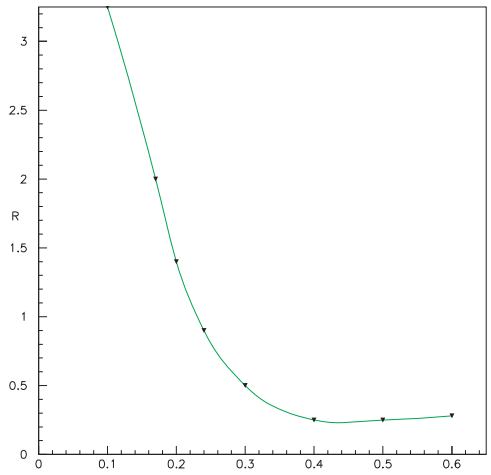

Fig. 20. – Variable R used by the CHARM collaboration *versus* $\sin^2\theta_w$: the big slope at values of $\sin^2\theta_w$ near 0.2 ensures the large sensitivity.

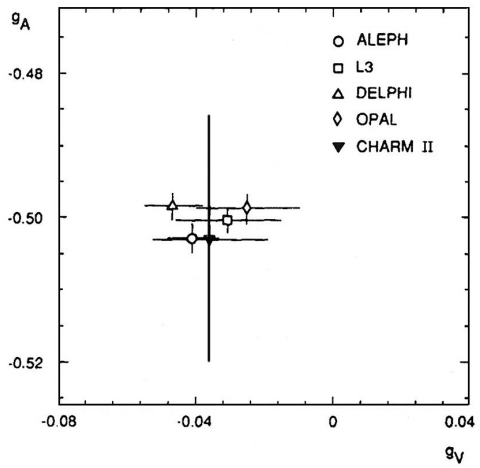

Fig. 21. – CHARM II and the 4 LEP experiments.

of particles produced inside it. The detector was exposed to the wide band beam at CERN. Neutrinos were produced by a 450 GeV proton beam of the SPS. The results in terms of g_V and g_A, compared with those of LEP, are reported in fig. 21 [95].

4·2.5. ν_e and $\overline{\nu}_e$ on electrons. The reactions $\nu_e + e \to \nu_e + e$ and $\overline{\nu}_e + e \to \overline{\nu}_e + e$ proceed both via the weak neutral and charged current and thus give rise to an interference term ($I1$). Table VI reports the experiments and their characteristics and fig. 22 illustrates the results in the (g_v, g_a)-plane (see fig. 10.1 in [132]).

Process 4) (see fig. 17) has been measured in the $\overline{\nu}_e$-beam at the Savannah River fission reactor and both 3) and 4) in an experiment at LAMPF. The results are collected in table VI. The interference term ($I1$) has been measured with the resulting values ($-1.07\pm$

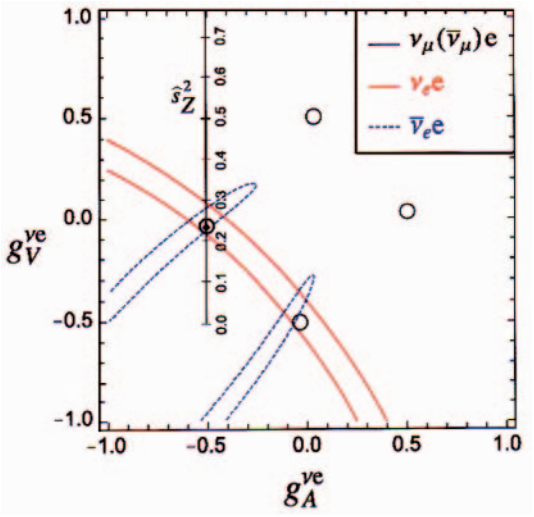

Fig. 22. – Contours in $g_A^{\nu e}$ and $g_V^{\nu e}$ and the S.M. best fit value $\sin^2\theta_w = 0.23116$.

0.21) [78] and (-1.01 ± 0.18) [79] demonstrating destructive interference consistent with SM prediction $I1 = -1.08$.

In the experiment at LAMPF (Clinton P. Anderson Meson Facility) the 800 MeV proton beam was stopped and the neutrinos are emitted isotropically in the π decay at rest. The spectra follow from the two-body $\pi^+ \to \mu^+ + \nu_\mu$ decay and the well-known three-body kinematics for $\mu^+ \to e^+ + \nu_e + \overline{\nu}_\mu$. Each stopped pion gives rise to a ν_e, to a ν_μ and to a $\overline{\nu}_\mu$. The events with a single e^- in the detector (a Liquid Scintillator Neutrino Detector-LSND) served to measure the total cross section. The authors of the experiments used: a) for sigma(NC) the best value of the corresponding cross section for muonic neutrino and b) sigma(CC) was determinad by the best value of the Fermi constant obtained from the muon decay. Using the best measurements of the cross sections σ(NC) and σ(CC) the interference term was extracted in a model-independent way, *i.e.* $I1 = \sigma_{\rm tot} - \sigma_{\rm NC} - \sigma_{\rm CC}$.

TABLE VI. – *Experiments devoted to the $\overline{\nu}_e$ and ν_e elastic scattering off e^-.*

Process	Exp./Ref.	E/MeV	N (ev)	σ (cm^2)$\cdot E_\nu$ (MeV) (for LAMPF)	$\sin^2\theta_w$
$\overline{\nu}_e^+ e^-$	Fission Reactor ref. [77]	1.5–3.0	-	$(0.87 \pm 0.25)\sigma_{V-A}$	0.29 ± 0.05
$\overline{\nu}_e^+ e^-$	ref. [77]	3.0–4.5		$(1.7 \pm 0.44)\sigma_{V-A}$	0.32 ± 0.05
$\nu_e e^-$	LAMPF [78] calorimeter 15 tons	$\simeq 31.7$	236 ± 35	$(10.0 \pm 1.5 \pm 0.9) * 10^{-45}$ $I1 = -1.07 \pm 0.21$	0.249 ± 0.063
$\overline{\nu}_e e^-$	LAMPF [79] Liq. Scint.+FC 167 tons	$\simeq 31.7$	191 ± 22	$(10.1 \pm 1.1 \pm 1.0) \cdot 10^{-45}$ $I1 = -1.01 \pm 0.18$	0.248 ± 0.051

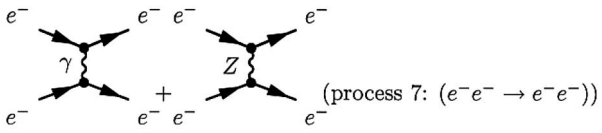

Fig. 23. – Moeller scattering (process 7)).

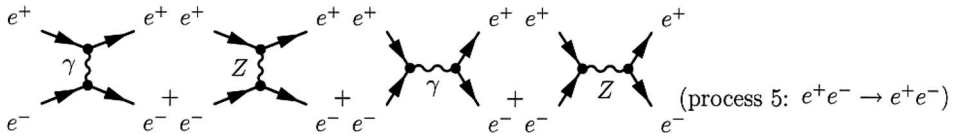

Fig. 24. – Bhabha scattering (process 5)).

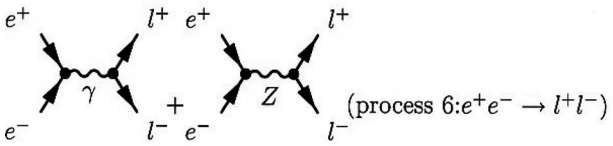

Fig. 25. – Lepton pair production in e^+e^- annihilation for $l \neq e$.

4˙2.6. Moeller scattering. The process $e^- + e^- \to e^- + e^-$, which is called *Moeller scattering*, has been studied at SLAC. Figure 23 shows the relevant Feynman graphs at tree level. The experiment consisted in the scattering of longitudinally polarized electrons on unpolarized targets (liquid H_2) and aimed at determining the parity-violating asymmetry $A_{\rm PV} = (\sigma_R - \sigma_L)/(\sigma_R + \sigma_L)$, where σ_R and σ_L are the cross sections for incident right- and left-handed electrons. $A_{\rm PV}$ arises from the interference $I2$ of the weak and electromagnetic amplitudes and is sensitive to the weak NC couplings, particularly to the weak mixing parameter $\sin^2\theta_w$. At the beam energy of $\simeq 50\,\text{GeV}$ at SLAC and the center-of-mass scattering angle of 90° $A_{\rm PV}$ in Moeller scattering was predicted to be $\simeq 320$ parts per billion (ppb) at tree level. The already tiny value got further reduced by electroweak radiative corrections and the experimental acceptance by more than 50%. This demonstrates the extraordinary sensitivity of the experiment. The result is shown in table VII.

TABLE VII. – *Experiment on Moeller scattering.*

Reaction	Exp./Ref.	Q^2/GeV^2	$A_{\rm PV}$	$\sin^2\theta_w$
$e^- + e^- \to e^- + e^-$	SLAC E158 [80]	0.026	$(-131 \pm 17)\cdot 10^{-9}$	0.2397 ± 0.0013

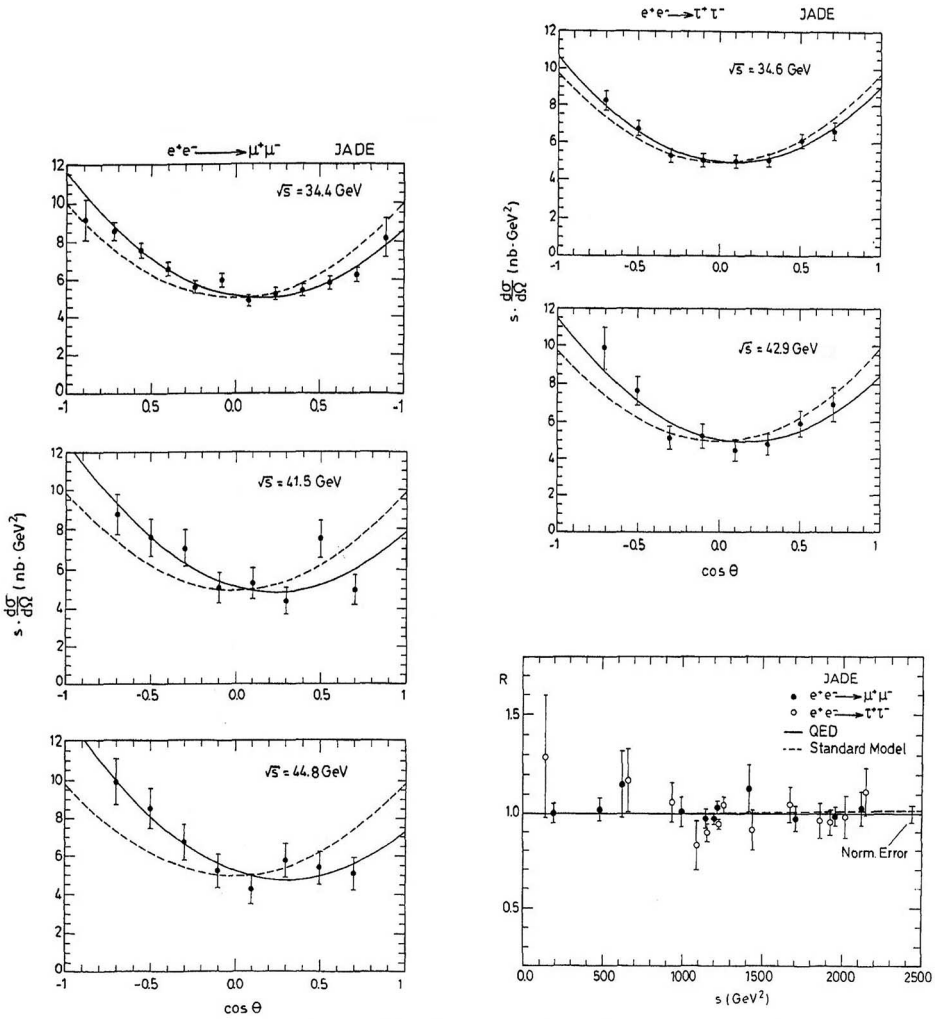

Fig. 26. – Angular asymmetry A and cross section ratio R for muons and taus from JADE; the solid (dashed) line is the Standard Model (QED) prediction.

4˙2.7. e^-e^+ below the Z pole. As mentioned above (see sect. **4**˙1.3) for center-of-mass energies below the mass M_Z the interference term between the electromagnetic and the weak amplitudes plays an important role. This was put in evidence at the 1981 Bonn Lepton-Photon Conference by combining the first PETRA data in the reaction $e^-e^+ \to \mu^-\mu^+$.

The experimental groups at PETRA (CELLO, JADE, MARKJ, PLUTO, TASSO), at PEP (HRS, MAC, MARKII) and later at TRISTAN (AMY, TOPAZ, VENUS) have systematically investigated the three lepton production processes $e^-e^+ \to l^-l^+$ for $l = e, \mu, \tau$ (see figs. 24, 25) providing information about the weak neutral current through the interference between the electromagnetic and the weak current. PEP was running at $\sqrt{s} = 29\,\text{GeV}$, PETRA covered the range 12–46.78 GeV, while TRISTAN extended it

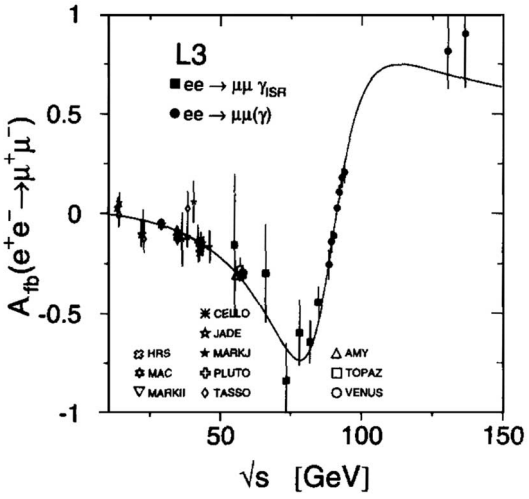

Fig. 27. – Energy dependence of the angular asymmetry A.

to the region 52–64 GeV. The measurement of the differential cross section $\mathrm{d}\sigma/\mathrm{d}\cos\theta$, where θ is angle between the incoming e^- and the outgoing l^-, provided information about the total cross section R and the angular asymmetry A, interpreted then in terms of the vector and axial-vector couplings of the leptons involved (ref. [26], p. 97). In this period complete calculations of radiative effects have been computed. In order to account for them assumptions had to be made about the Z-mass, known then to 1–2 GeV, while the masses of the top quark and the Higgs boson were not yet known. All participating groups measured the differential cross sections of lepton production. For illustration some distributions are shown by the JADE collaboration in fig. 26. It is interesting to note that the total cross section ratio remains well described by QED alone in the PETRA energy regime despite the non-trivial presence of weak effect. Figure 27 shows the onset

TABLE VIII. – *Experiment JADE at PETRA.*

Final state	$\lvert a_l\rvert$	$\lvert v_l\rvert$
$e^- + e^+$	$0.48^{+0.14}_{-0.27}$	0.15 ± 0.17
$\mu^- + \mu^+$	0.58 ± 0.06	0.16 ± 0.17
$\tau^- + \tau^+$	$0.44^{+0.09}_{-0.11}$	$0.26^{+0.09}_{+0.14}$

TABLE IX. – *All experiments at PETRA and PEP* [96].

Laboratory	s (GeV)^2	$4a_e * a_\mu$	$4a_e * a_\tau$
PEP	841	0.99 ± 0.12	0.88 ± 0.16
PETRA Low energies	1190	1.26 ± 0.15	0.87 ± 0.31
PETRA High energies	1880	1.09 ± 0.16	0.87 ± 0.25

of the weak interactions in the asymmetry as measured by the PEP and PETRA groups as a function of the center-of-mass energy. The measurements were continued by the TRISTAN collaborations demonstrating the increasing importance of the weak relative to the electromagnetic amplitude. At still higher energies the asymmety goes through a minimum and then rises towards the Z-resonance. This regime could be mapped out at LEP by exploiting the process $e^+e^- \to \mu^+\mu^-\gamma$ with a hard photon in the final state, as measured for instance by the L3 group between 50 and 80 GeV (ref. [101], see also fig. 15). The Standard Model describes quantitatively the data.

The interference terms in the quantities A and R in l^+l^- production are proportional to $a_e a_l$ and $v_e v_l$, as evident from the formulae in sect. **4**˙1. Therefore, no sign information on a_l and v_l is possible. Results on the couplings are reported in tables VIII and IX.

The average from all PEP and PETRA data yielded $\langle v_e v_l \rangle = 0.028 \pm 0.019$ (ref. [26], p. 146) to be compared with the expected value 0.04 of the Standard Model. As a consequence the cross section ratio R_l remains well described by QED alone (see fig. 26). Table IX summarizes the measurements of the axial-vector couplings constants from PETRA (CELLO, MARKJ, PLUTO, JADE and TASSO) and PEP (HRS, MAC and MARK II).

Charged lepton universality is confirmed to better than two standard devations. For further details refer to the reviews [46-50].

4˙2.8. e^-e^+ around the Z-pole. Z-decays are an ideal place to study the weak neutral current. The differential cross sections of the processes $e^+e^- \to f\overline{f}$ have been investigated at Stanford by the SLD collaboration and at Geneva by the four LEP collaborations ALEPH, DELPHI, L3, OPAL at and around the Z-pole (for details see ref. [52]). The formula at Born level including the beam polarization is

$$\frac{\mathrm{d}\sigma_f}{\mathrm{d}\cos\theta} = \frac{3}{8}\sigma_f^{\mathrm{tot}}[(1 - P_e A_e)(1 + \cos^2\theta) + 2(A_e - P_e)A_f \cos\theta], \tag{12}$$

where P_e is the electron beam polarization and A_f is the asymmetry parameter of the fermion with flavour f. The formula in sect. **4**˙1 is reproduced for $P_e = 0$. The asymmetry is given in terms of the weak couplings by

$$A_f = \frac{2a_f v_f}{a_f^2 + v_f^2}\,.$$

The total cross section at the Z-pole (index 0) is

$$\sigma_f^0 = \frac{12\pi\Gamma_f^2}{M_Z^2\Gamma_Z^2}\,.$$

With σ_F and σ_B being the integrals over the forward and backward hemispheres, various asymmetries can be formed:

– The Forward-Backward asymmetry: $A_{FB} = \frac{\sigma_F - \sigma_B}{\sigma_F + \sigma_B}$,

– The Left-Right asymmetry: $A_{LR} = \frac{\sigma_L - \sigma_R}{\sigma_L + \sigma_R}\frac{1}{\langle|P_e|\rangle}$,

– The combined asymmetry: $A_{LRFB} = \frac{(\sigma_F - \sigma_B)_L - (\sigma_F - \sigma_B)_R}{(\sigma_F + \sigma_B)_L + (\sigma_F + \sigma_B)_R}\frac{1}{\langle|P_e|\rangle}$.

TABLE X. – *Partial widths (unit: MeV).*

$\Gamma_{\rm had}$	Γ_{ee}	$\Gamma_{\mu\mu}$	$\Gamma_{\tau\tau}$	$\Gamma_{\rm inv}$
1745.8 ± 2.7	83.92 ± 0.12	83.99 ± 0.18	84.08 ± 0.22	499.0 ± 1.5

The lepton aymmetries provided the cleanest and most precise measurements of $\sin^2\theta_w$ (see fig. 29).

Assuming lepton universality, the leptonic pole cross section was measured to be

$$\sigma^0_{\rm lep} = \frac{12\pi\Gamma^2_{ll}}{M^2_Z\Gamma^2_Z} = 2.0003 \pm 0.0027\,{\rm nb},$$

in excellent agreement with the S.M. expectation [81].

The partial Z decay widths are reported in table X; the invisible width calculated from $\Gamma_{\rm inv} = \Gamma_Z - (\Gamma_{\rm had} + \Gamma_{ee} + \Gamma_{\mu\mu} + \Gamma_{\tau\tau})$ is also shown and represents the partial decay width of Z into three neutrino species. The lepton universality is well established.

By using these data, the LEP collaborations were able to determine the number of the neutrino families to be [81]

$$N_\nu = 2.9841 \pm 0.0083.$$

The polarised electron beams at SLAC allowed the SLD collaboration [82] to measure the asymmetry parameter A_l directly by analysing the left-right and the left-right forward-backward asymmetry, $A^0_{LR} = A_e$ and $A^0_{LRFB} = (3/4)A_l$. The analysis of the τ polarisation and its forward-backward asymmetry at LEP yielded A_τ and A_e separately. The forward-backward pole asymmetries $A^{0,l}_{FB} = (3/4)A_eA_l$ constrain the product of two

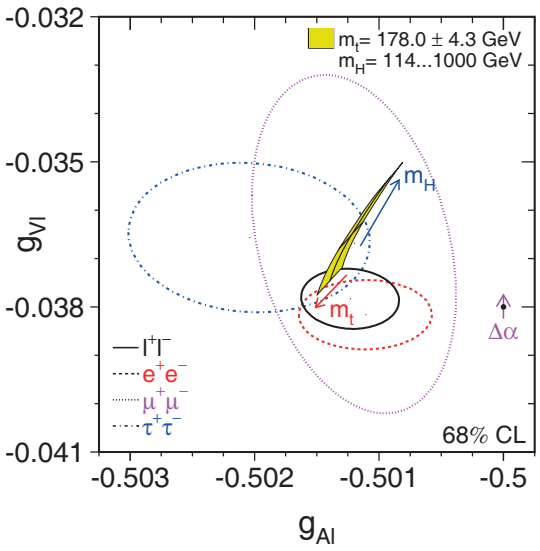

Fig. 28. – Final leptonic coupling constants from SLD and LEP-1 [102].

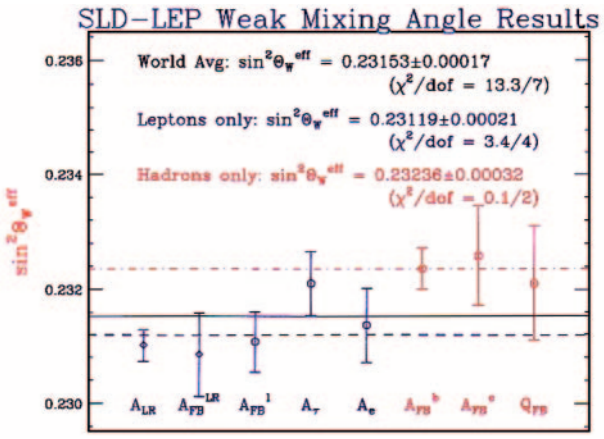

Fig. 29. – Comparison of $\sin^2\theta_w$ from measurements at the Z-pole [129].

asymmetry parameters. The measurements were performed separately for all the three charged leptons channels. The measured forward-backward asymmetries gave the following results: $A^e_{FB} = 0.0145 \pm 0.0025$, $A^\mu_{FB} = 0.0169 \pm 0.0013$ and $A^\tau_{FB} = 0.0188 \pm 0.0017$. The results on the leptonic asymmetry parameters are reported in table XI.

TABLE XI. – *Leptonic asymmetry parameters A_l.*

Parameters A_l [132]	from $A^{0,l}_{FB}$	from A^0_{LR}, A^l_{LRFB}	from P_τ
A_e	0.139 ± 0.012	0.1516 ± 0.0021	0.1498 ± 0.0049
A_μ	0.162 ± 0.019	0.142 ± 0.015	-
A_τ	0.180 ± 0.023	0.136 ± 0.015	0.1439 ± 0.0043

TABLE XII. – *Leptonic coupling constants from LEP and SLC (see also fig. 28).*

a_e	a_μ	a_τ	$a_\nu = v_\nu$
v_e	v_μ	v_τ	–
-0.50112 ± 0.00015	-0.50115 ± 0.00056	-0.50204 ± 0.00064	$+0.50068 \pm 0.00075$
-0.0378 ± 0.0011	-0.0376 ± 0.0031	-0.0368 ± 0.0011	–

The asymmetry parameters A_l determine the ratio v_l/a_l([2]) of the effective vector and axial-vector coupling constants, while the partial dacay widths of the Z boson determine the sum of the squares of the these two coupling constants. The expressions for both observables are invariant under the exchange $v \leftrightarrow a$, thus fixing only the relative sign of A_l. The v, a ambiguity is resolved making use of the sign convention $a < 0$. In table XII their measured values are reported.

([2]) Equivalent notations for the vector and axial-vector couplings are in use: (v_f, a_f) or (g^f_V, g^f_A), where f is the flavour index.

Figure 28 illustrates the final results on the vector and axial-vector couplings together with their dependence on the top and Higgs masses. In fig. 29 [129] are reported the values of $\sin^2\theta_w$ measured at the Z-pole, where 5 refer to leptonic and 3 to hadronic final states. The corresponding world average from SLD and LEP are also shown. While the overall remarkably precise world average is 0.23153 ± 0.00017, the separate averages for the leptons 0.23119 ± 0.00021 and hadrons 0.23236 ± 0.00032 appear to differ 3.2 standard deviations.

4˙3. *Semileptonic interactions.* – An abundant amount of data exists on this subject. In order to extract the relevant information on the elementary processes it was mandatory to take into account the nucleon structure [51]. The experiments on lepton-nucleon scattering provided information both on the nucleon structure and on the structure of the electroweak interaction. Therefore, the available knowledge, which was poor at the beginning of the '70s, slowly improved and rendered the quark parton model more and more powerful. An irreducible source of systematic uncertainty is related to the distinction of long- and short-range processes. Some stability was only achieved, when higher-order QCD processes became available. These problems are, of course, absent in the case of purely leptonic reactions.

It is appropriate to recognize the enormous work accomplished with the Bubble Chamber technique. Pioneering work started in the 1960's with the NPA 1.2 m heavy liquid bubble chamber exposed to the ν and $\overline{\nu}$ beams of the CERN PS in the new energy region 1–10 GeV. In this and the subsequent period larger bubble chambers were operating: the 12 foot bubble chamber at Argonne (ANL), the 7 foot bubble chamber at Brookhaven (BNL), the 15 foot Bubble chamber at Fermilab, Gargamelle and the Big European Bubble Chamber (BEBC) at CERN, the Serpukov bubble chamber SKAT. They were used to study neutrino and antineutrino interactions off free and bound nucleons and were covering energies from 0.5 up to a few 100 GeV. Until the 1980s the bubble chambers made unique contributions to the understanding of weak, but also strong, interactions by investigating in detail exclusive and inclusive processes. The virtue of bubble chambers consisted in providing in-depth information about the final state, *i.e.* precise vertex information and flavour composition of the final state particles. Two outstanding examples from Gargamelle are the full reconstruction of the process $\nu + n \to \nu + n + \pi^0$ (see fig. 41) consisting of neutrals only and $\nu + p \to \mu^- + \Sigma_c^{++}$ with the complete reconstruction of the charmed barion (see fig. 30). The bubble chamber technique remained competitive until the mid of the 1980s, when electronic detectors with refined calorimeters, vertex detectors, track chambers and fast data acquisition became superior and took the lead.

The experimental data have been grouped in the following categories:

- inclusive processes on isoscalar targets (nuclei such as carbon, iron, etc.),
- inclusive processes on non-isoscalar targets (protons and neutrons),
- exclusive processes: elastic scattering, single π production, deuteron break-up ($\overline{\nu}_e + D \to \overline{\nu}_e + n + p$), coherent production of π^0 on nuclei, etc.,
- atomic parity violation.

Other semileptonic processes leading to hadronic final states, in particular the intensive investigation of heavy flavours in e^+e^- interactions, as well as semileptonic data from hadron colliders [130] have not been considered, apart from a few remarks.

4˙3.1. Inclusive processes on isoscalar targets. Figure 31 shows a prominent candidate for a deep inelastic neutral current interaction in the bubble chamber Gargamelle. All

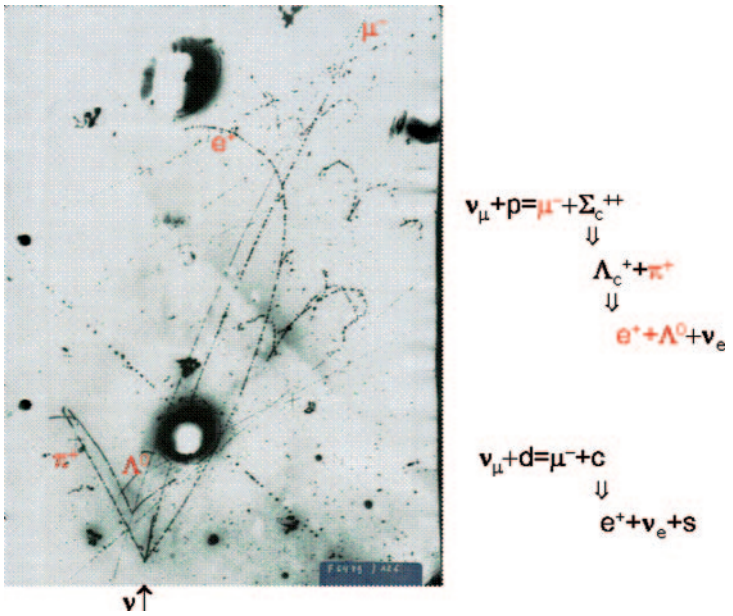

Fig. 30. – Neutrino-induced Σ_c^{++} production observed in Gargamelle.

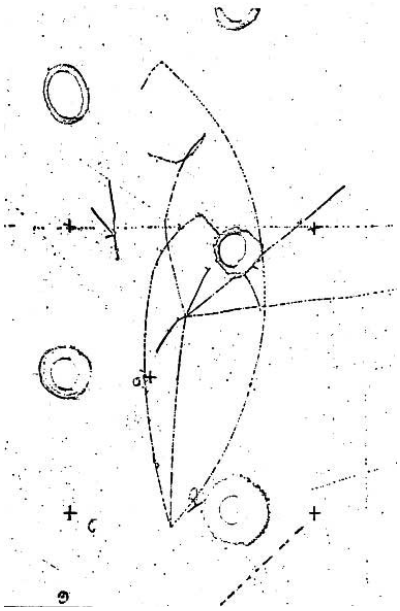

Fig. 31. – Neutral-current candidate observed in Gargamelle. The neutrino beam enters from below. All secondaries are identified as hadrons.

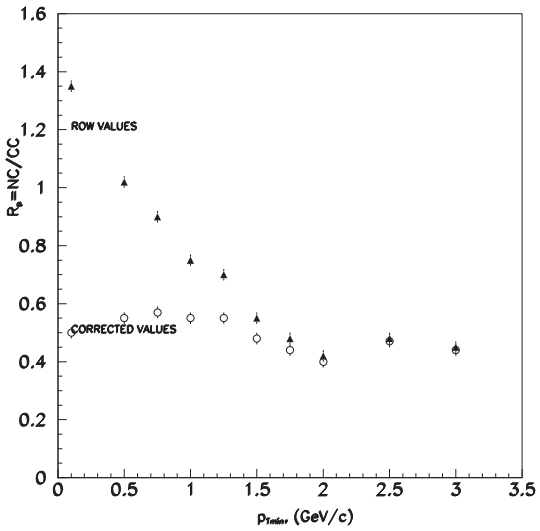

Fig. 32. – Neutrons and neutrinos in BEBC.

tracks can be followed until a visible interaction occurs, thus ensuring that the tracks are due to charged hadrons.

The measured quantities were the neutral- and charged-current-induced total cross sections in either wide band or narrow band ν and $\overline{\nu}$ beams. In order to reduce the sensitivity to the nucleon structure functions the following ratios were considered:

$$R_\nu = \frac{\sigma^{\mathrm{NC}}(\nu N)}{\sigma^{\mathrm{CC}}(\nu N)}\,,$$

$$R_{\overline{\nu}} = \frac{\sigma^{\mathrm{NC}}(\overline{\nu} N)}{\sigma^{\mathrm{CC}}(\overline{\nu} N)}\,.$$

Besides the ratios R_ν and $R_{\overline{\nu}}$ of the inclusive neutral- and charged-current cross sections for ν and $\overline{\nu}$ also the following ratios, proposed by Pascos and Wolfenstein [98], have been studied:

$$R_+ = \frac{\sigma^{\mathrm{NC}}(\nu N) + \sigma^{\mathrm{NC}}(\overline{\nu} N)}{\sigma^{\mathrm{CC}}(\nu N) + \sigma^{\mathrm{CC}}(\overline{\nu} N)}\,, \tag{13}$$

$$R_- = \frac{\sigma^{\mathrm{NC}}(\nu N) - \sigma^{\mathrm{NC}}(\overline{\nu} N)}{\sigma^{\mathrm{CC}}(\nu N) - \sigma^{\mathrm{CC}}(\overline{\nu} N)}\,. \tag{14}$$

Equation (13) describes the total strength of the NC coupling, while eq. (14) is sensitive to the $V-A$ interference. For instance, $u_R = d_R = 0.$ implies pure $V-A$; $u_L = d_L = 0.$ implies $V+A$; $u_L = u_R$ pure V and $d_L = d_R$ pure A.

For the separation of neutral-current from charged-current-induced events the bubble chambers had to deal with the notorious neutron problem, which was considerably improved by equipping them with electronic devices (External Muon Identifier (EMI) and Internal Picket Fence (IPF)). The calorimeter experiments applied the event length

TABLE XIII. – *Measurements of R_{ν_μ} and $R_{\overline{\nu}_\mu}$.*

Exp./Ref.	Target	R_{ν_μ}	$R_{\overline{\nu}_\mu}$	Hadr. Energy cut (GeV)
GGM-PS [69]	Freon	0.26 ± 0.04	0.29 ± 0.06	0.
HPWF-FNAL [72]	CH_2	0.30 ± 0.04	0.33 ± 0.09	0.
CITF-FNAL [126]	Iron	0.28 ± 0.03	0.35 ± 0.11	12.
CHARM-SPS [124]	marble	0.320 ± 0.010	0.377 ± 0.020	2.
BEBC-SPS [125]	H_2-Ne	0.345 ± 0.015	0.364 ± 0.029	9.
CDHS-SPS [123]	iron	0.300 ± 0.007	0.357 ± 0.015	10.
BEBC-SPS [121]	D_2	0.33 ± 0.02	0.35 ± 0.04	5.
FNAL-15 ft [119, 120]	D_2	0.30 ± 0.03	-	5.

technique pioneered by the CITF group, see for instance fig. 33. Precise measurements of the NC and CC cross section ratios R_ν and $R_{\overline{\nu}}$ came from the counter experiments CDHS and CHARM at CERN, CCFR and NuTeV in the USA. A selection of R_{ν_μ} and $R_{\overline{\nu}_\mu}$ measurements is reported in table XIII. A more complete collection can be found in table 6.46 of ref. [26].

Figure 32 illustrates the behaviour of the neutron background in BEBC with H_2 filling. For the first experiments at the SPS the collaborations of the bubble chamber BEBC and the new calorimeter CDHS were equally fast in evaluating and publishing their data, however this changed quickly in favour of the electronic detectors. BEBC filled with a mixture of Ne-H_2 (75 mole%Ne corresponding to an average proton/neutron ration of 1.07) [99, 125] contributed with their data obtained in the 200 GeV/c narrow band beam at CERN one of the first precise values of the weak angle: $\sin^2\theta_w = 0.182 \pm 0.020 \pm 0.012$.

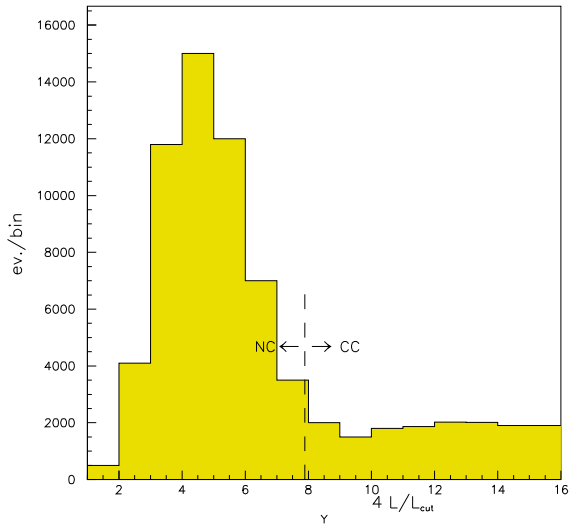

Fig. 33. – Observed event length distribution. Events in the peak are dominantly originating from neutral-current interactions, while charged-current events generate a rather flat distribution.

In a workshop organized by the SPS Committee 1981 the question was posed, whether the 1-loop radiative effects could be detected in neutrino experiments. The Born level value of $\sin^2\theta_w$ shifts by 0.01, when radiative corretions are taken into account. It turned out that the present precision was insufficient, but that it may be possible in a high statistics exposure with improved systematic uncertainties. This program was successfully carried out and both CDHS [90] and CHARM [91] reached the required experimental precision of ± 0.005 (see also sect. **4**˙3.3).

4˙3.2. Inclusive processes on protons and neutrons. Meaurements on free protons and quasifree neutrons were the privilege of bubble chambers filled with hydrogen, deuterium and propane:

– CERN: BEBC with H_2 and D_2 filling [70, 121, 122] WBB.
– CERN: BEBC with a TST(H_2) filling [73, 74] surrounded by Ne-H_2 mixture.
– FNAL: 15 ft with H_2 filling [71].

The results are reported in table XIV.

As outlined in sect. **3**˙2 the Lagrangian for low-energy neutrino-quark interactions, written for u and d quarks, takes on the simple form

$$\mathcal{L}(\nu q) = \frac{G}{\sqrt{2}} J_\nu (u_L J_L^u + u_R J_R^u + d_L J_L^d + d_R J_R^d), \tag{15}$$

where $u_{L,R}$ and $d_{L,R}$ are the chiral coupling constants of the u and d quark. In the case of an isoscalar target one obtains for the neutral-to-charged cross section ratio R

$$R_\nu = (u_L^2 + d_L^2) + r(u_R^2 + d_R^2) + \text{corrections},$$
$$R_{\overline{\nu}} = (u_L^2 + d_L^2) + \frac{1}{r}(u_R^2 + d_R^2) + \text{corrections},$$

TABLE XIV. – *Measurements on protons and neutrons.*

Exp./Ref.	Target	$R^p_{\nu_\mu}$	$R^n_{\nu_\mu}$	$R^p_{\overline{\nu}_\mu}$	$R^n_{\overline{\nu}_\mu}$
15 ft [120, 119]	D_2	0.49 ± 0.06	0.22 ± 0.03	-	-
BEBC [121]	D_2	0.49 ± 0.05	0.25 ± 0.02	0.26 ± 0.04	0.57 ± 0.09
BEBC [122]	D_2	0.41 ± 0.03	0.24 ± 0.02	0.30 ± 0.04	0.49 ± 0.06
BEBC [70]	H_2	0.51 ± 0.04	-	-	-
15 ft [73, 74]	H_2	0.48 ± 0.17	-	0.36 ± 0.06	-
BEBC-TST [71]	H_2	0.47 ± 0.04	-	0.33 ± 0.04	-

TABLE XV. – *Chiral couplings from inclusive measurements on isoscalar targets.*

Exp./Ref.	$(u_L^2 + d_L^2)$	$(u_R^2 + d_R^2)$	$\sin^2\theta_w$
BEBC [122]	0.301 ± 0.025	0.022 ± 0.018	0.247 ± 0.029
CDHS [123]	0.300 ± 0.015	0.022 ± 0.008	0.232 ± 0.012
CHARM [124]	0.305 ± 0.013	0.036 ± 0.013	0.220 ± 0.014
CITFRR [126]	0.292 ± 0.020	0.038 ± 0.020	0.242 ± 0.016
Average	0.301 ± 0.009	0.028 ± 0.006	0.231 ± 0.008

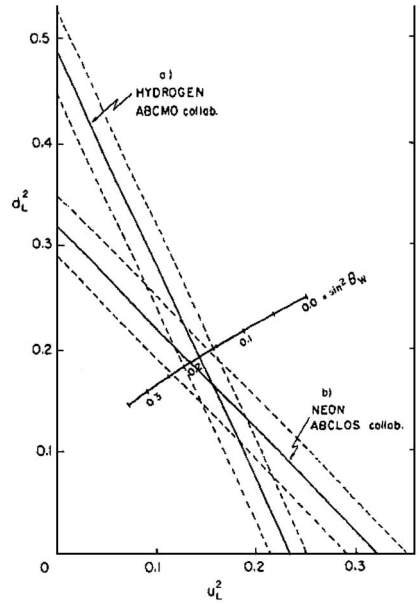

Fig. 34. – Left-handed (u, d) couplings constrained by two in BEBC experiments.

where $r = (\sigma_{\overline{\nu}}/\sigma_\nu)_{CC} = \frac{\overline{q}+q/3}{q+\overline{q}/3}$ (q =quark distribution function). Thus, measurements on isoscalar targets only contrain the sums $u_L^2 + d_L^2$ and $u_R^2 + d_R^2$. Results are collected in table XV. Already after the first years of investigating the structure of weak neutral

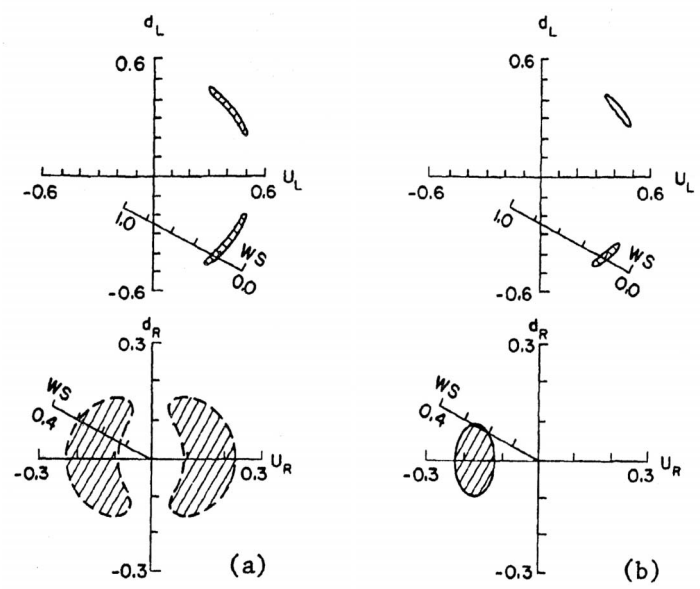

Fig. 35. – Constraining the (u_L, d_L)- and (u_R, d_R)-planes: (a) inclusive on isoscalar and non-isoscalar targets, (b) all interactions with hadrons; WS = Standard Model [75].

currents the attention turned to proposals on measuring the differences $u_L^2 - d_L^2$ and $u_R^2 - d_R^2$. The most direct way [109,110] would consist in measuring

$$\frac{\sigma(\nu p) - \sigma(\nu n)}{\sigma(\nu p) + \sigma(\nu n)} \quad \text{and} \quad \frac{\sigma(\overline{\nu} p) - \sigma(\overline{\nu} n)}{\sigma(\overline{\nu} p) + \sigma(\overline{\nu} n)},$$

since the nominators are proportional, respectively, to $u_L^2 - d_L^2 + \frac{1}{3}(u_R^2 - d_R^2)$ and $u_R^2 - d_R^2 + \frac{1}{3}(u_L^2 - d_L^2)$. In practice, the information on the differences was obtained by combining measurements on proton targets and isoscalar targets for ν and $\overline{\nu}$.

As an example, the authors of [70] found $R_p = 0.51 \pm 0.04$ and combining with the values of R^ν measured in neon and in hydrogen (see fig. 34) they obtained $u_L^2 = 0.15 \pm 0.05$ and $d_L^2 = 0.17 \pm 0.07$. Figure 35 [127] illustrates the situation around 1981. The data leave two solutions. Only the dominant isovector solution is consistent with the Standard Model. This is confirmed by the analysis of the single pion data (see sect. **4**˙3.5) excluding a pure isoscalar contribution, as well as by the study of the reaction $\overline{\nu}_e D \to np\overline{\nu}_e$. The ultimate analysis including all neutrino data up to 1988 is presented in the next section.

4˙3.3. Combination of all inclusive neutrino data. The investigation of the inclusive ν- and $\overline{\nu}$-induced processes occurred in the period when important aspects of the electroweak theory were still in progress. As a consequence each publication between 1973 and 1988 contained assumptions, which represented the knowledge at the time of publication, but which changed subsequently. In order to fully exploit the valuable information in these experiments an attempt was made [51] to put them all on the same footing with regard to the experimental conditions (kinematic cuts, choice of phenomenological paramters such as the masses of W, Z, *top*) and to the structure of the nucleon. In this way it was possible to demonstrate the shift due to radiative effects and to obtain the most precise model-independent infomation on the left- and right-handed u and d couplings. Their sums $g_L^2 = u_L^2 + d_L^2$ and $g_R^2 = u_R^2 + d_R^2$ and differences $\delta_L^2 = u_L^2 - d_L^2$ and $\delta_R^2 = u_R^2 - d_R^2$, are reported in table XVI together with the corresponding correlations matrices.

TABLE XVI. – *The chiral couplings.*

Coupling	Value	Errors	
		Exp.	Sys.
g_L^2	0.2982	0.0028	0.0029
g_R^2	0.0309	0.0034	0.0028
δ_L^2	−0.0588	0.0233	0.0042
δ_R^2	0.0206	0.0155	0.0037

$$\begin{pmatrix} 1 & -0.715 & -0.100 & 0.118 \\ & 1 & 0.064 & 0.097 \\ & & 1 & -0.436 \\ & & & 1 \end{pmatrix} \pm \begin{pmatrix} 1 & -0.914 & -0.975 & 0.606 \\ & 1 & 0.945 & -0.677 \\ & & 1 & -0.712 \\ & & & 1 \end{pmatrix}.$$

Since $\delta_{L,R}^2$ is constrained by $\pm g_{L,R}^2$ the impact coming from the non-isoscalar data can be illustrated as the restricted area inside the square formed by $|\delta_L^2| < g_L^2$ and $|\delta_R^2| < g_R^2$, as also seen in fig. 36. The results are also illustrated in figs. 37, 38.

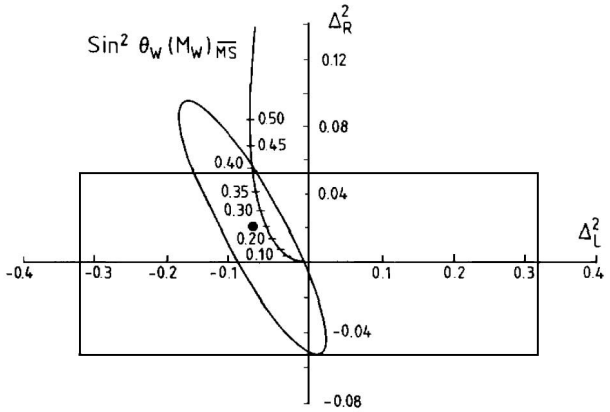

Fig. 36. – The impact of Bubble chambers (note: $\Delta_{L,R}$ stands for $\delta_{L,R}$ in the text).

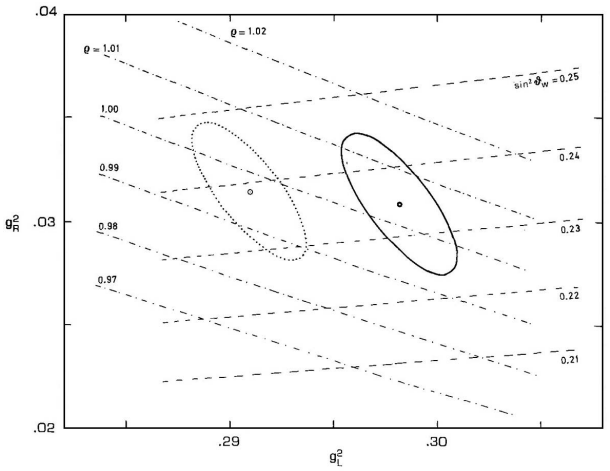

Fig. 37. – The chiral couplings $g^2_{R,L}$. The ellipse with the thick line corresponds to the 1-loop level, while the dotted one to the Born level, demonstrating the importance of weak radiative effects.

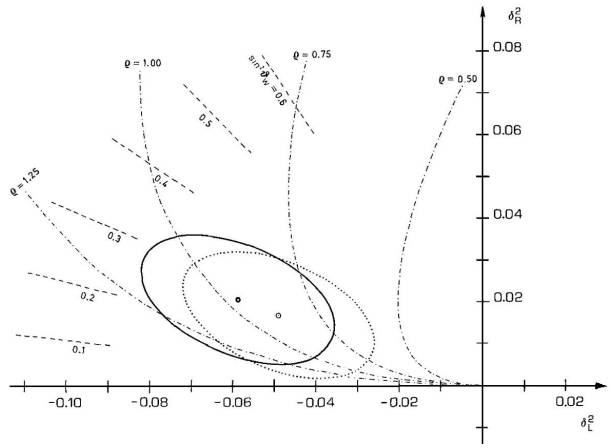

Fig. 38. – The chiral couplings $\delta^2_{R,L}$. The shift due to radiative effects is much less pronounced than of $g^2_{R,L}$ in fig. 37.

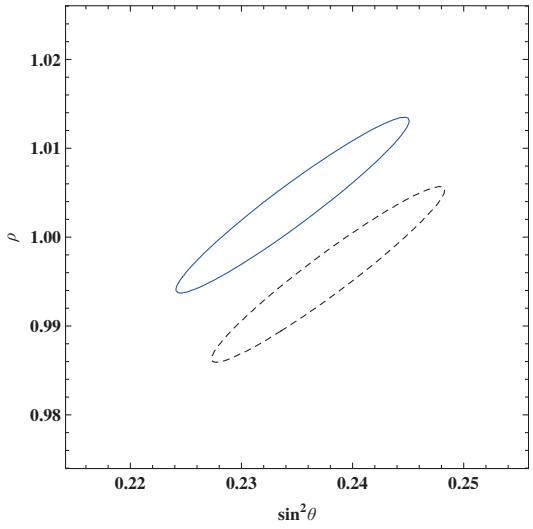

Fig. 39. – Two-parameter fit.

The calorimeter experiments dominated the determination of the $g_{L,R}$, while the differences $\delta_{L,R}$ were achieved by the bubble chamber experiments.

The two-parameter fit in fig. 39 shows clearly the sensitivity to 1-loop corrections. The resulting value for $\sin^2\theta_w$ within the Minimal Standard Model is

$$\sin^2\theta_w = 0.2309 \pm 0.0029 \pm 0.0024$$

and is the most precise value of $\sin^2\theta_w$ from the neutrino sector.

4˙3.4. Elastic scattering. Elastic neutrino-nucleon scattering via the weak neutral current is a fundamental probe of the nucleon. The reactions of the type $\nu N \to \nu N$, in the case of carbon $\nu\text{Nucleus}(C) \to \nu\text{Nucleus}(C)$, may be viewed as scattering off individual nucleons or from collective nuclear effects.

The process on carbon should be sensitive to the nucleon isoscalar weak currents as opposed to charged-current quasielastic scattering which interacts only via isovector weak currents. Many experiments were performed in the past in ν and $\overline{\nu}$ beams. Their results are reported in table XVII.

One of the highest statistics measurements was performed in the mid-1980s at BNL using a 170 ton liquid scintillator detector in ν and $\overline{\nu}$ beams [76] (BNL E734). They have collected 1686 $\nu p \to \nu p$ and 1821 $\overline{\nu} p \to \overline{\nu} p$ and measured the differential cross section as a function of the four-momentum transfer squared (Q^2). The MiniBooNE experiments [105, 106] have reported the most recent data on the ratio NCE/CCQE of the neutral-current elastic to the charged-current quasielastic cross sections.

Usually, elastic neutral- and charged-current processes are described by dipole form factors similarly to the photon-induced lepton-nucleon reactions. This suggests to assume an approximate isospin rotation invariance for the components of the $I = 1$ part of the weak current. The $I = 0$ part of the weak current is assumed to behave analogously.

Figure 40 shows the observed differential distribution for the elastic ν and $\overline{\nu}$ NC

TABLE XVII. – *Ratio of elastic NC over quasielastic CC cross sections for ν and $\overline{\nu}$.*

Experiment	Ref.	R_ν^{el}	$R_{\overline{\nu}}^{\mathrm{el}}$
HPB	[97]	0.11 ± 0.02	0.19 ± 0.025
CIR	[103]	0.20 ± 0.06	-
AP	[87]	0.10 ± 0.03	-
GGM	[104]	0.12 ± 0.06	-

processes [73]. Defining the form factors

$$G_E(Q^2) = g_V(Q^2) - \left(\frac{Q^2}{2M^2}\right) f_V(Q^2), \tag{16}$$

$$G_M(Q^2) = g_V(Q^2) + f_V(Q^2) \tag{17}$$

in the matrix element

$$\langle p'|J(\mathrm{NC})|p\rangle = \overline{u}(p')[\gamma_\lambda g_V(Q^2) + i(\sigma_{\lambda,\alpha}/2M)q^\alpha f_V(Q^2) + \gamma_\lambda\gamma_5 g_A(Q^2)]u(p) \tag{18}$$

and assuming that G_M, G_E and g_A have the same Q^2 dependence as their charged-current counterparts (dipole form factor with $M_V^2 = 0.84\,\mathrm{GeV}^2$ and $M_A^2 = 0.90\,\mathrm{GeV}^2$), a fit to the differential cross section yields at $Q^2 = 0$

- $G_E = 0.5^{+0.25}_{-0.5}$,
- $G_M = 1.0^{+0.35}_{-0.40}$,
- $g_A = 0.5^{+0.20}_{-0.15}$.

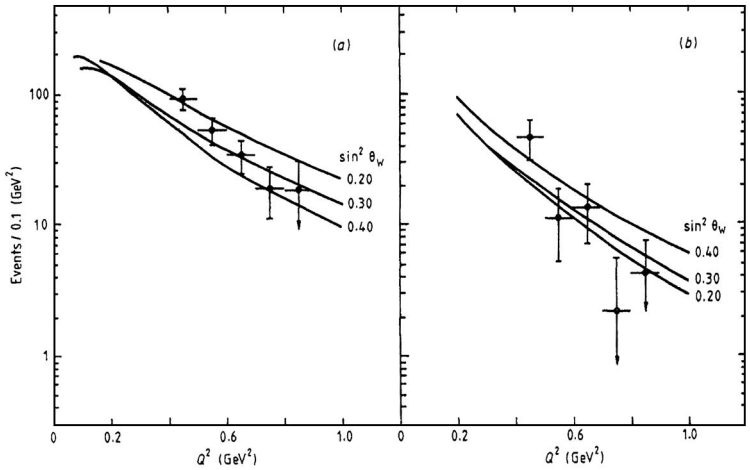

Fig. 40. – Observed differential NC cross sections for neutrinos (a) and antineutrinos (b), see [100].

A fit to the Standard Model yields [97] $\sin^2\theta_w = 0.26 \pm 0.04$.

4˙3.5. Single-pion production. The first exclusive neutral-current process was observed in 1974 at Argonne [23]. A systematic study of all 4 channels was carried out in Gargamelle filled with propane and freon mixture [112, 115] exposed to the CERN PS neutrino and antineutrino beams

$$\nu(\overline{\nu}) + p \to \nu(\overline{\nu}) + p + \pi^0,$$
$$\nu(\overline{\nu}) + p \to \nu(\overline{\nu}) + n + \pi^+,$$
$$\nu(\overline{\nu}) + n \to \nu(\overline{\nu}) + p + \pi^-,$$
$$\nu(\overline{\nu}) + n \to \nu(\overline{\nu}) + n + \pi^0.$$

A real challenge was the detection of the final state consisting of a neutron and a π^0, both neutral, hence leaving no track in the bubble chamber. The final state can nevertheless be reconstructed through the observed secondaries of the interacting neutron and the decay of the π^0 into two photons observed as two gamma pairs. An example is shown in fig. 41.

Single-pion production is an ideal source for testing the isospin properties of the weak neutral current [116]. Gargamelle was filled with a propane and freon mixture [112,115], see also [26] p. 157. Propane (C_3H_8) has free and bound protons, thus allowing interesting studies of nuclear effects, particularly in the channel with a single final state π^0. As seen in fig. 11 a clear enhancement shows up at the position of the $\Delta(1236)$ resonance. This was the first observation of a resonance excited by the weak neutral current. The reaction occurs both on free and bound protons. The implications of resonance production has

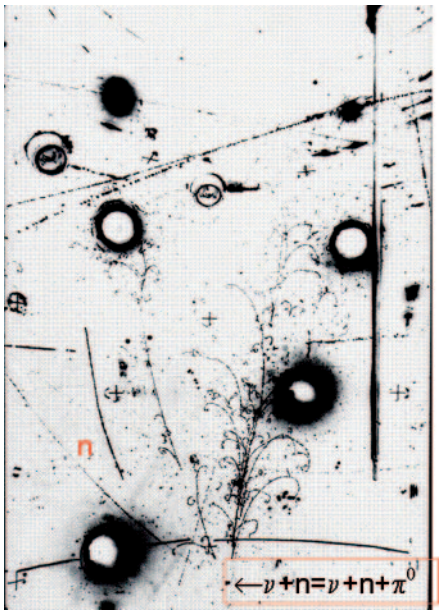

Fig. 41. – Candidate for $\nu n \to \nu n \pi^0$.

been studied by two groups [107, 108].

Some important results are

$$\frac{\sigma(\nu N \to \nu\pi^0 N')}{\sigma(\nu N \to \nu\pi^- N')} = 1.4 \pm 0.2,$$
$$\frac{\sigma(\overline{\nu} N \to \overline{\nu}\pi^0 N')}{\sigma(\overline{\nu} N \to \overline{\nu}\pi^- N')} = 2.1 \pm 0.4.$$

If neutral currents were purely isoscalar, then the cross sections off neutrons and protons should be equal, namely 0.9 in contrast to observation, since then only a $I = 1/2$ final state is produced. Thus the hypothesis of a pure isoscalar can be ruled out, as already obvious by the mere observation of the Δ resonance. The conclusion, that a dominant isovector contribution appears in this channel, is confirmed in the reaction [111]

$$\overline{\nu}_e + d \to \overline{\nu}_e + p + n$$

with the data collected by the Irvine group using the intense flux of $2.5 \times 10^{13}\,\mathrm{cm}^{-2}\,\mathrm{s}^{-1}$ of $\overline{\nu}_e$ from the Savannah River fission reactor. Near the threshold the final (np) system is in a ^1S state. The transition from the ^3S of the deuteron to the ^1S can only occur via the isovector axial-vector part of the transition Lagrangian. The cross section $(3.8 \pm 0.9)\,10^{-45}\,\mathrm{cm}^2$ was measured consistent with the dominant isovector solution of neutral-current coupling $\sigma_{\mathrm{exp}}/\sigma_{\mathrm{th}} = 0.8 \pm 0.2$ and excluding a dominant isoscalar solution. The experiment directly determined the isovector axial-vector coupling constant [113]: $|\beta| = 0.9 \pm 0.1$. The parameter β is related to the chiral couplings as follows: $\beta = u_L - u_R - d_L + d_R$=1.

In a common effort the ν and $\overline{\nu}$ Gargamelle collaborations have determined the single π^0 total cross sections and found that their difference is non-vanishing (see sect. **4**˙1.1).

The measurements of the inclusive and exclusive semileptonic channels have been used also to explore the Lorentz nature of the weak neutral current. The results shown in ref. [128] and fig. 42 prove that the NC interactions are not of the pure $V - A$ form as CC interactions, but have also a non-trivial $V + A$ contribution. In conclusion, the properties of the weak neutral current regarding its Lorentz and isospin structure are in agreement with the Standard Model and imply $\sin^2\theta_w = 0.227 \pm 0.006$.

4˙4. *Atomic parity violation.* – Parity was assumed to be a fundamental symmetry of nature, until in the year 1956 T. D. Lee and C. N. Yang expressed some doubts about the conservation of parity in weak interactions. Already a year later C. S. Wu demonstrated in her famous experiment that parity is indeed violated in weak interactions and even maximally violated. This was achieved by studying the ^{60}Co beta decay and paved the way towards the $V - A$ theory.

At the end of the '60s and during the '70s many experiments were performed to find out, whether parity violation also existed in atoms [59]. Here the situation was different as opposed to beta decay. An atom exhibits a high degree of symmetry and it is dominated by electromagnetic interactions which conserve parity. Experiments at the beginning did not find any sign of such effects. A new situation occurred with the advent of the Glashow-Salam-Weinberg model and the discovery of the weak neutral current in Gargamelle. Now an interference between the electromagnetic and the weak neutral current should induce parity-violating effects. The relevant amplitudes differ in atoms by many orders of magnitude. Systematic searches in this field started in 1973 at the

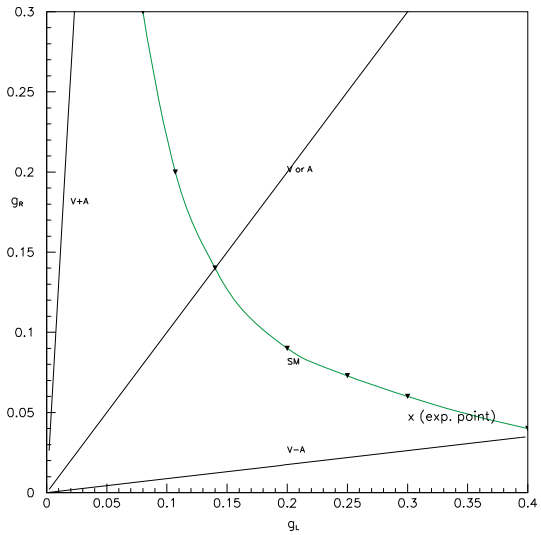

Fig. 42. – The measured chiral coupling (cross) is compared with the prediction of the Standard Model (green line) and the prediction assuming various combinations of vector and axial-vector currents ($V + A$, $V - A$ and $V = A$).

Ecole Normale Superieur (for a review see [59, 61]). There are fortunately some effects that enhance the PV effects in nuclei

- the growth of the asymmetry in heavy atoms (faster than Z^3) [62],
- it is possible to work on highly forbidden transitions where $A_{\rm em}$ is strongly inhibited.

In September 1979 the communities of the Atomic Physicists and High Energy Physicists met at Cargèse [60] and conluded at the end of the conference that the first observation of parity-violating effects in atoms was established at a statistical level corresponding to 2-3σ. The first positive result on Cs that became in the following years at the level of 6σ, was reported in 1982 [59, 64]. In fig. 43 [59] are reported the two parameters C_u and C_d determining the parity-violating effect of Cs and also elastic scattering of the polarized electrons on deuterium obtained at SLAC at higher energy.

Figure 44 shows the cesium energy levels and the relevant transitions. The parity-violating interaction mixes a small amount of the P states into the states $6S$ (ground state) and $7S$ of Cs; this gives rise to an electric dipole ($E1$) transition amplitude $E1_{pv}$, between these S states. The measurements of the interference with some other process (for instance the Stark effect induced by a strong electric field E) open the possibility to measure the ratio of the parity non-conserving amplitude to the vector transition polarizability β ($E_{pnc} = 1.5935 \pm 0.0056\,\mathrm{mV/cm}$). The parity violation in atomic physics is usually written in the non-relativistic limit as follows:

$$V_{pv} = \frac{G_F}{\sqrt{2}} \frac{Q_w \delta^3(r_e) \vec{s}_e \vec{p}_e}{4 m_e c} \,. \tag{19}$$

The various quantities are: The Fermi coupling constant G_F, the weak charge of the nucleus Q_w, the δ function taking account of the large mass of the Z^0 and the short range of its interaction, s_e spin and p_e momentum of the electron.

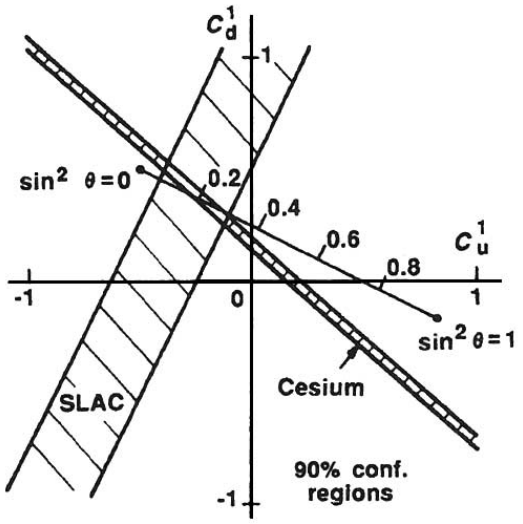

Fig. 43. – Impact of Cs experiments and the *ed* experiment (SLAC) in the (C_u, C_d)-plane (for APV see [131]).

The magnitude of $E1_{pv}$ depends not only on Q_w but also on the atomic factor involving the atomic wave functions of the nucleus. Therefore an atomic calculation is required to extract Q_w from $E1_{pv}$ which implies another source of uncertainty on the measured Q_w. The progress in evaluating the parity-violating amplitude is reported in fig. 45. The best value of the weak charge for ^{133}Cs is [65]

$$Q_w = -73.16 \pm 0.29 \pm 0.20,$$

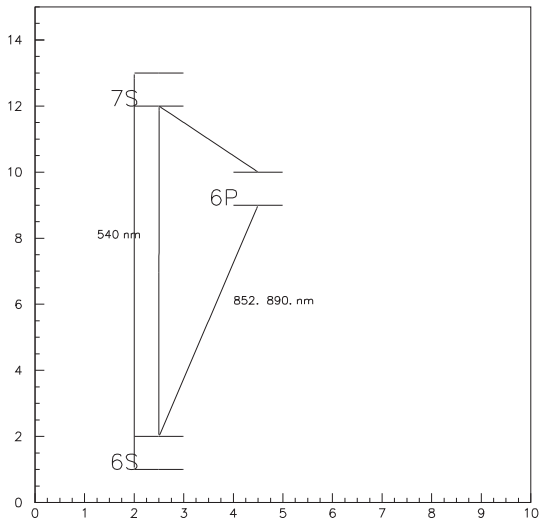

Fig. 44. – Cs levels.

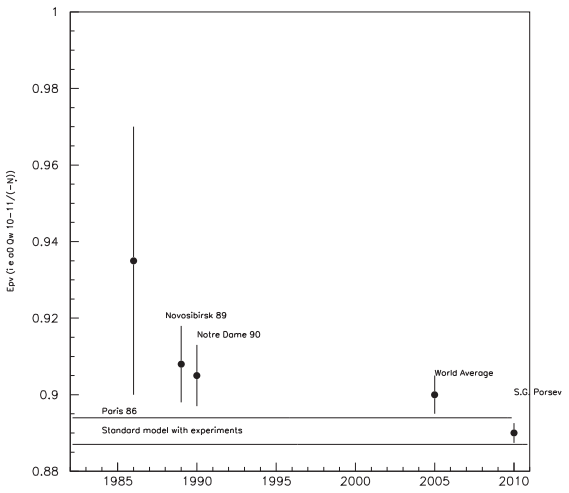

Fig. 45. – Progress.

where the first uncertainty is experimental and the second one theoretical. This value agrees well with the prediction of the Standard Model [65]:

$$Q_w = -73.16 \pm 0.03.$$

The corresponding value of the mixing parameter is

$$\sin^2 \theta_w(E \to 0) = 0.2381 \pm 0.0011.$$

See also the previous results on Cs in [66, 67].

4˙5. *Summary and outlook.* – The experiments at accelerators and colliders during the past four decades following the discovery of weak neutral currents have established their properties at the per mille precision in agreement with the electroweak gauge theory. A clear picture emerged. The precision achieved so far has not given any hint for new physics, apart from two discrepancies at the level of three standard deviations

– $\sin^2 \theta_w$ from asymmetries with leptons and heavy quarks disagree as seen in fig. 29.

– $\sin^2 \theta_w$ from Nutev:

  The NuTeV collaboration [118] has reported a determination of $\sin^2 \theta_w$ in the on-shell scheme: $0.2277 \pm 0.0013(\text{stat}) \pm 0.0009(\text{syst})$ [132]. This value is 3 standard deviations above the Standard Model value 0.2227 ± 0.0003. It is an open debate whether this discrepancy is to be taken as a sign for new physics or rather as an indication of a not understood aspect in the interpretation of the data.

New experiments to measure $\sin^2 \theta_w$ at various values of Q^2 have been proposed:

– An Ultra-precise Measurement of the mixing weak angle using Moeller scattering: E12-09-005 December 2, 20010 Jefferson Lab.

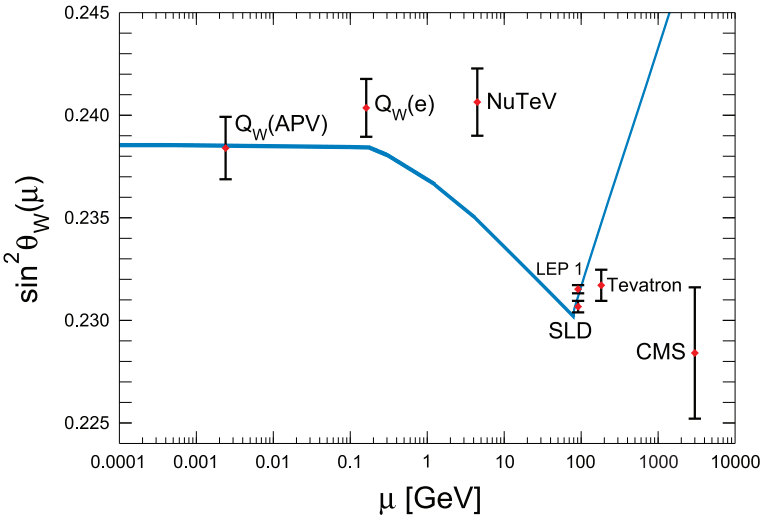

Fig. 46. – Running of $\sin^2\theta_w$ in the $\overline{MS}$ renormalization scheme.

– Atomic Parity NON conservation in francium; the Fr PNC experiment at TRIUMF.

– From Hadronic Parity Violation to Electron Parity-Violating experiments W.T.H. van Oers ISS June 2-5 TAIPEI.

Their expected precision should come near to the one obtained by LEP-I at the Z-pole. Precise low-energy measurements remain an invaluable tool to learn about the scale of new physics and to shed light onto the flavour sector. Their virtue consists in the sensitivity to the presence of corrections affecting vacuum polarization of the intermediate vector bosons (γ, Z and W) through new particles in quantum loops, vertices and boxes. Figure 46 summarizes the presently most precise data [132]. At the high-energy frontier the LHC experiments will elucidate the Higgs sector and search for new physics. While the mass of the Higgs boson was previously inferred from the result of fitting all eletroweak quantities, $M_h = 99^{+28}_{-23}$ GeV [132], now its value is actually measured. This new information completes the on-shell renormalization scheme and allows to predict any electroweak quantity within the minimal SM. In particular, a global fit [133] to the mixing angle $\sin^2\theta^{\rm lept}_{\rm eff}$ yields

$$\sin^2\theta^{\rm lept}_{\rm eff} = 0.23150 \pm 0.00010.$$

The main contributions to the error are 0.000030 from the top quark mass, 0.000035 from $\Delta\alpha_{\rm had}$ and 0.000047 from theory. In this fit all quantities sensitive to the weak angle are excluded, such that it can be directly compared with value obtained from the measured Z-asymmetries (see fig. 29)

$$\sin^2\theta^{\rm lept}_{\rm eff} = 0.23153 \pm 0.00017.$$

Good agreement is found. The electroweak theory is valid to better than 10^{-3}.

5. – The impact of neutral currents

The discovery of weak neutral currents represents a milestone in elementary particle physics. It is the key to the unification of the two previously independent fields, electromagnetism and weak interactions. The immense impact since 1973 over the following four decades until the present elucidation of the Higgs sector stands out manifestly.

The discovery of weak neutral currents has given substance to the Glashow-Salam-Weinberg model and paved the way towards the Standard Model of electroweak interactions. For a long time the only quantum theory was quantum electrodynamics (QED) based on the local gauge theory $U(1)$. Now in the larger gauge group $SU(2) \times U(1)$ there are three intermediate gauge bosons: the photon mediating electromagnetic interactions, the $W^{\pm}$ mediating the weak Fermi (or charged-current) interactions and the Z mediating the weak neutral-current interactions. The structural link is the gauge principle. A new feature is that these bosons interact with each other in contrast to QED as a consequence of the non-Abelian algebraic structure of the underlying gauge group. The masses of the weak bosons set the scale for a precise meaning of the terms *low* and *high energy* physics. In fact, the weak phenomena previously described within the Fermi $V-A$ theory are reproduced as the *low energy* limit of the embracing electroweak theory, *i.e.* Q^2 and $s \ll M_W^2$; similarly, the predictions by QED remain good provided the relevant invariants Q^2 and s remain sufficiently small(see [26], p. 93).

Weak neutral currents were a driving force on all frontiers. Right after their discovery all major laboratories have re-evaluated their scientific goals and set up a long-range program. The following remarks may give a flavour.

5˙1. *Fundamental scientific frontier*. – The discovery in neutrino physics has opened the new field of neutrino interactions mediated by the Z-boson. The next important step was to demonstrate the (γ, Z)-interference and parity violation. This inspired the elegant electron-deuteron experiment at SLAC [57] and opened a new field in atomic physics with a series of experiments reaching eventually high precision. The challenging character of these experiments consisted in getting access to the tiny admixture of weak effects in the presence of the overwhelming dominance of electromagnetic interactions. Only two decades later the *ep*-collider HERA provided the possibility to study in the space-like regime both weak and electromagnetic effects on equal footing.

Weak neutral currents brought an intense boost [55] to astrophysics. Already a year after the discovery Schramm and Arnett [54] recognized their key role particularly for the understanding of stellar collapse. In addition to the known W-induced processes now many more Z-induced processes are contributing. The annihilation of e^+e^- pairs into a neutrino pair generates neutrinos of *all* flavours and acts as an efficient new mechanism of cooling in supernovae and elsewhere. Another key role of neutrinos in astrophysics is related to their large mean free path, thus carrying away energy from the core of stellar objects. With the detection of neutrinos from the Supernova SN1987a and the observation of neutrino oscillations a new field, neutrino astronomy, was born.

Weak neutral currents also entered biology. Chiral asymmetry shows up in biomolecules and suggested a relation to parity violation in weak charged and neutral currents (see, for instance, [56]).

5˙2. *Technology and energy frontiers*. – The investigation of the properties of weak neutral currents has influenced major developments. An immediate requirement was to gather large and pure samples of neutrino-induced neutral-current events. High statistics

was achieved by building detectors with large target mass (in addition to Gargamelle, BEBC, the 15 foot and 12 foot bubble chambers, then the new detectors CDHS, CHARM, CCFR, Nutev) and by building new higher-energy proton synchrotrons and boosters (the CERN SPS, the FNAL Main Ring Synchrotron), since the event rate is proportional to the target mass and to the neutrino energy. Pure samples required good discrimination against background. This led to bubble chambers equipped with electronic devices and to counter experiments with fine granularity. The development of calorimeters was important for the future collider experiments. These detectors were truly omnipurpose instruments. With their increasing size also the collaborations building and exploiting them got larger and larger. The latest generation at the LHC involves more than 2000 members in a collaboration. The increasing complexity is also a challenge for computing, detector simulation, data acquisition and processing.

In a workshop organized by the SPSC in 1981 [58] the question was discussed whether the neutrino experiments at CERN can be improved to measure the shift in $\sin^2\theta_w$ due to electroweak effects. This meant to reduce the uncertainty in $\sin^2\theta_w$ to the unprecedented precision of ± 0.005. The collaborations CDHS and CHARM indeed reached the required precision in measuring the inclusive NC/CC ratio. In addition, CHARM also obtained this precision in neutrino electron scattering with neutrino and antineutrino sample of order 1000. The bubble chambers, specially when filled with hydrogen or deuterium, remained for some time competitive and could obtain unique results. Neutrino physics reached the stage of precision physics, but the time of fixed target experiments touched at its end and a new era with colliders was beginning.

The frustrating search for the intermediate vector boson W in neutrino experiments since 1963 resulted in steadily increasing mass limits without any sign of existence, until the weak neutral currents offered a new clue. The GSW model relates the mass of the weak bosons with $\sin^2\theta_w$. Using the early measurements of $\sin^2\theta_w$ it became obvious that the W had to have a mass of order 70 GeV, thus beyond the reach of neutrino experiments. Cline, Rubbia and McIntyre [45] reported to the Neutrino Conference at Aachen 1976 the idea to detect the weak bosons in a proton-antiproton collider. This experiment was realized at CERN by adding to the SPS an antiproton accumulator ring. The two collaborations UA1 and UA2 have observed in 1983 for the first time the weak bosons W and Z and investigated in the following years their properties.

The quest for higher and higher energies moved from fixed target experiments at accelerators and to omnipurpose experiments at colliders: e^+e^- (PETRA/PEP(1978), TRISTAN(1986), SLC/LEP(1993)), $p\overline{p}$ ($S\overline{p}pS$(1981), Tevatron(1983)) and ep (HERA(1992)) and recently to pp (LHC(2008)). In this way the electroweak force was explored at ever smaller distances. The interplay of experiment and theory allowed to pin down the elusive Higgs boson to a small energy interval around 125 GeV. LHC, the Large Hadron Collider, built to either prove its existence or to definitely rule it out, announced in July 2012 the discovery of a resonance at 125 GeV in agreement with the properties of the Standard Model Higgs boson.

* * *

It is a pleasure to thank Prof. L. Cifarelli, president of the Italian Physical Society, and her Scientific Committee for confering to us the prestigious Fermi Prize 2012. We also thank Prof. A. Bettini for the opportunity to revive the exciting times of the discovery and to review its impact during the past four decades. We appreciate his forbearance while waiting for the completion of the manuscript.

REFERENCES

[1] Fermi E., *Z. Phys.*, **88** (1934) 161.
[2] Nguyen-Khac U. and Lutz A. M. (Editors), *Proceedings of the International Conference on Neutral Currents 20 years later, Paris July 6-9, 1993* (World Scientific) 1994.
[3] Perkins D. H., *Gargamelle and the Discovery of Neutral Currents*, *Proceedings of the Third International Symposium on the History of Particle Physics, SLAC 24-27 June, 1992* (Cambridge University Press) 1997.
[4] Mann A. K. and Cline D. B. (Editors), *Discovery of Weak Neutral Currents: The Weak Interaction Before and After, International Symposium on the Discovery of Weak Neurtal Current, AIP Conf. Proc.*, Vol. **300** (American Institute of Physics) 1994.
[5] Cashmore R., Maiani L. and Revol J. P., *Prestigious Discoveries at CERN, Eur. Phys. J. C*, **34** (2004) 1.
[6] Brianti G., *CERN's contribution to accelerators and beams* in ref. [5].
[7] Lee T. D., *Phys. Rev. Lett.*, **4** (1960) 307.
[8] Gargamelle, ν-proposal CERN TCC/70-12 (1970).
[9] Hasert F. J. *et al.*, *Phys. Lett. B*, **46** (1973) 138.
[10] Hasert F. J. *et al.*, *Phys. Lett. B*, **46** (1973) 121.
[11] Puliia A., *Invited Talk at the Conference of the Società Italiana di Fisica (SIF), Florence, September 1973*.
[12] Haidt D., *Note on Pullia's method*, GGM internal note February 25th 1974.
[13] Pullia A., *Riv. Nuovo Cimento*, **7**, N. 2 (1984).
[14] Fry W. F. and Haidt D., CERN Yellow Report 75-1 (1975) 1.
[15] Haidt D., *Observation of hadronic weak neutral currents in Gargamelle - Solving the neutral hadron background problem* in [2], pp. 69-92.
[16] Haidt D., Precision of neutrino beam, CERN TC-L (1971).
[17] Eichten T. *et al.*, *Nucl. Phys. B*, **44** (1972) 333.
[18] Wachsmuth H., *Nucl. Phys. B (Proc. Suppl.)*, **36** (1994) 401.
[19] Haidt D., Contribution to the APS Meeting at Washington, April 1974.
[20] Perkins D. H., Memo to the Gargamelle Collaboration, April 14, 1972.
[21] Rousset A., *Détermination de la contribution des neutrons dans les candidats courants neutres hadroniques*, CERN Report, TC-L/AR/ft (1973, 8 March).
[22] Pullia A., in *Proceedings of the XVII International Conference on High Energy Physics London, July 1974* (Science Research Council) 1974.
[23] Barish S. J. *et al.*, contribution to the APS Meeting at Washington, April 1974; *Phys. Rev. Lett.*, **33** (1974) 1454.
[24] Barish B., contribution to ref. [22].
[25] Benvenuti A. *et al.*, *Phys. Rev. Lett.*, **32** (1974) 800.
[26] Haidt D. and Pietschmann H, *Landolt-Börnstein New Ser.* **I/10** (1988).
[27] Veltman M., *About the Genesis of the Standard Model*, in ref. [2] pp. 151-165.
[28] Weinberg S., *The making of the Standard Model*, in ref. [5].
[29] Weinberg S., *Rev. Mod. Phys.*, **52** (1980) 515.
[30] Glashow S. L and Iliopoulos J. and Maiani L., *Phys. Rev. D*, **2** (1970) 1285.
[31] 't Hooft G., *Nucl. Phys. B*, **33** (1971) 173; *Nucl. Phys. B*, **35** (1971) 167.
[32] 't Hooft G. and Veltman M., *Nucl. Phys. B*, **44** (1972) 189.
[33] Hasert F. J. *et al.*, *Nucl. Phys. B*, **73** (1974) 1.
[34] Pullia A., *Observation of hadronic weak neutral currents in the Gargamelle experiment*, in *Proceedings of the International Conference: Neutral currents twenty years later*, in ref. [2] pp. 55-66.
[35] Langacker P., *Advanced Series on Directions in High Energy Physics*, Vol. **14** (World Scientific) 1995.
[36] Schaile D. and Zerwas P. M., *Phys. Rev. D*, **45** (1992) 3262.
[37] Zerwas P. M., *W & Z physics at LEP* in ref. [5].
[38] Darriulat P., *The discovery of the W & Z, a personal recollection* in ref. [5].

[39] Chaichian M. and Nelipa N. F., *Texts and Monographs in Physics* (Springer-Verlag) 1984.
[40] Bettini A., *Introduction to Elementary Particle Physics* (Cambridge University Press) 2008.
[41] Fukugita M. and Yanagita T., *Physics of Neutrinos and Applications to Astrophysics* in *Texts and Monographs in Physics* (Springer-Verlag) 2003.
[42] Veltman M., *Facts and Mysteries in Elementary Particle Physics* (World Scientific) 2003.
[43] Hagiwara K., Haidt D., Kim C. S. and Matsumoto S, *Z. Phys. C*, **64** (1994) 559.
[44] Hagiwara K., Haidt D. and Matsumoto S., *Eur. Phys. J. C*, **2** (1998) 95.
[45] Cline D., Rubbia C. and McIntyre, *Proceedings of the International Neutrino Conference Aachen 1976*, edited by Faissner H., Reithler H. and Zerwas P. (Friedr. Vieweg & Sohn) 1977, p. 683.
[46] Naroska B., *Phys. Rep.*, **148** (1987) 67.
[47] Wu Sau- Lan, *Phys. Rep.*, **107** (1984) 216.
[48] Lohrmann E., *Review of e^+e^- Physics at PETRA*, *DESY*, **83-102** (1983) .
[49] Duinker P., *Rev. Mod. Phys.*, **54** (1982) 325.
[50] Sakuda M., *Nuovo Cimento A*, **107** (1994) 2389.
[51] Fogli G. L. and Haidt D., *Z. Phys. C*, **40** (1988) 379.
[52] Electroweak Working Group CERN, *Phys. Rep.*, **427** (2006) 257-454; hep-ep/0509008.
[53] Kodama K. *et al.*, *Phys. Lett. B*, **504** (2001) 218.
[54] Schramm D. and Arnett W. D., *Astrophys. J.*, **198** (1974) 629.
[55] Freedman D. Z. and Schramm D. and Tubbs D. L., *The weak neutral current and its effects in stellar collapse Annu. Rev. Nucl. Sci.*, **27** (1977) 167.
[56] Kondepudi D. K. and Nelson G. W., *Nature*, **314** (1985) 438.
[57] Prescott C. Y. *et al.*, *Phys. Lett. B*, **77** (1978) 524.
[58] Haidt D., SPS Fixed Target Workshop at Cogne 1981, CERN Report 82-02 (1983).
[59] Bouchat M. A., arXiv:1111.2172v1 [physics.atom-ph] 9 Nov 2011.
[60] Williams W. L. (Editor), *Proceedings of the International Workshop on Neutral Current Interaction in Atoms, Cargèse, September 1979*, (Paris) 1980.
[61] Bouchiat M. A. and Pottier L., *J. Phys. (Paris)*, **37** (1976) L79.
[62] Bouchiat M. A. and Bouchiat C., *Phys. Lett. B*, **48** (1974) 111; *J. Phys. (Paris)*, **35** (1974) 899; *J. Phys. (Paris)*, **37** (1975) 493.
[63] Bouchiat M. A. and Pottier L., *Science*, **234** (1986) 1203.
[64] Bouchiat M. A. *et al.*, *Phys. Lett. B*, **117** (1982) 358; *Phys. Lett. B*, **134** (1984) 463; *J. Phys. (Paris)*, **46** (1985) 1897; *J. Phys. (Paris)*, **47** (1986) 1175; *J. Phys. (Paris)*, **47** (1986) 1709.
[65] Porsev S. G. *et al.*, *Phys. Rev. Lett.*, **102** (2009) 181601.
[66] Wood C. S. *et al.*, *Science*, **275** (1977).
[67] Bennet S. C. and Wieman C. E., *Phys. Rev. Lett.*, **82** (1999) 2484.
[68] Amser C., *Phys. Lett. B*, **667** (1) 2008.
[69] Blietschau J. *et al.*, *Nucl. Phys. B*, **118** (1977) 218.
[70] Blietschau J. *et al.*, *Phys. Lett. B*, **88** (381) 1979.
[71] Armenise N. *et al.*, *Phys. Lett B*, **122** (1983) 448.
[72] Wanderer P. *et al.*, *Phys. Rev. D*, **17** (1978) 1679.
[73] Harris F. *et al.*, *Phys. Rev. Lett.*, **39** (1977) 437.
[74] Carmony D. D. *et al.*, *Phys. Rev. D*, **26** (1982) 2965.
[75] Winter K., *Proceedings of the Sixth International Symposion on Electron and Photon Interactions at High Energies* (Fermilab) 1980, 253.
[76] Ahrens L. *et al.*, *Phys. Rev. D*, **34** (1986) 75.
[77] Reines F. *et al.*, *Phys. Rev. Lett.*, **37** (1976) 315.
[78] Allen R. C. *et al.*, *Phys. Rev. D*, **47** (1993) 11.
[79] Auerbach L. B. *et al.*, *Phys. Rev. D*, **63** (11201) .
[80] Anthony P. L. *et al.*, *Phys. Rev. Lett*, **95** (2005) 081601.

[81] LEP Collaboration, CERN-EP/2003-091, hep-ex/0312023 (2003).
[82] SLD collaboration, SLAC-PUB-8029, Dec (1998).
[83] Blietschau J. *et al.*, *Nucl. Phys. B*, **114** (1976) 189.
[84] Blietschau J. *et al.*, *Phys. Lett. B*, **73** (1978) 232.
[85] Faissner H. *et al.*, *Phys. Lett. B*, **68** (1977) 377.
[86] Faissner H. *et al.*, *Phys. Rev. Lett.*, **41** (1978) 213.
[87] Faissner H. *et al.*, *Phys. Rev. D*, **21** (1980) 555.
[88] Cnops A. M. *et al.*, *Phys. Rev. Lett.*, **41** (1978) 357.
[89] Armenise N. *et al.*, *Phys. Lett. B*, **86** (1979) 225.
[90] Abramowicz H. *et al.*, *Phys. Rev. Lett.*, **57** (1986) 298.
[91] Allaby J. V. *et al.*, *Phys. Lett. B*, **77** (1986) 446.
[92] Abe K. *et al.*, *Phys. Rev. Lett.*, **62** (1989) 1709.
[93] Ahrens L. A. *et al.*, *Phys. Rev. D*, **41** (1990) 3297.
[94] Baker N. J. *et al.*, *Phys. Rev. D*, **40** (1989) 2753.
[95] Akkus B. *et al.*, *Nucl. Phys. B*, **31** (1993) 287.
[96] Bartel W. *et al.*, *Z. Phys. C*, **30** (1986) 371.
[97] Entenberg A. *et al.*, *Phys. Rev. Lett.*, **42** (1979) 1198.
[98] Pascos E. A. and Wolfenstein L., *Phys. Rev. Lett.*, **7** (1973) 91.
[99] Deden H. *et al.*, *Nucl. Phys. B*, **149** (1979) 1.
[100] Myatt G., *Rep. Prog. Phys.*, **45** (1982) 1.
[101] Acciari M. *et al.*, *Phys. Lett. B*, **374** (1996) 289.
[102] LEP EWWG, `http://lepewwg.web.cern.ch/LEPEWWG/plots/zpole_2005`.
[103] Lee W. *et al.*, *Phys. Rev. Lett.*, **37** (1977) 186.
[104] Pohl M. *et al.*, *Phys. Lett. B*, **728** (1978) 489.
[105] Aguillar-Arvalo A. *et al.*, *Phys. Rev. D*, **79** (2009) 072002.
[106] Aguillar-Arvalo A. *et al.*, *Phys. Rev. D*, **82** (2010) 092005.
[107] Fogli G. L. and Nardulli G., *Nucl. Phys. B*, **160** (1989) 116.
[108] Rein D. and Sehgal L. M., *Ann. Phys.*, **113** (1981) 79.
[109] Sehgal L. M., CERN/SPSC 78-153, SPSC/G 22-12-1978.
[110] Amaldi U., *International Conference on Neutrino Physics, Bergen* Vol. I, (June 1979) p. 367.
[111] Pasierb E. *et al.*, *Phys. Rev. Lett.*, **43** (1979) 96.
[112] Krenz W. *et al.*, *Nucl. Phys. B*, **135** (1978) 45.
[113] Sakurai J. J., *International Conference on Neutrino Physics, Bergen, 1979* UCLA/79/TEP/15 (1979).
[114] Haidt D., *Proceedings of the International (Ben Lee Memorial) Conference on Parity Nonconservation, Weak Neutral Current and Gauge Theories, FNAL 1977*, edited by Cline D. and Mills F. (Harwood Academic Publishers) 1977, p. 77.
[115] Bertrand-Coremans G. *et al.*, *Phys. Lett. B*, **61** (1976) 207.
[116] Fogli G. L., *Nucl. Phys. B*, **165** (1980) 162.
[117] Altarelli G. and Grunewald M. W., *Phys. Rep.*, **403-404** (2004) 189.
[118] Zeller G. P. *et al.*, *Phys. Rev. Lett.*, **88** (2002) 091802 and Erratum ibid. **90** (2003) 239902; arXiv:hep-ex/0110059.
[119] Kafka T. *et al.*, *Phys. Rev. Lett.*, **48** (1982) 910.
[120] Merriner J. *et al.*, *Phys. Rev. D*, **27** (1983) 2569.
[121] Allasia D. *et al.*, *Phys. Lett. B*, **133** (1983) 129.
[122] Allasia D. *et al.*, *Nucl. Phys. B*, **307** (1988) 1.
[123] Geweniger G., in *Proceedings of HEP83: International Europhysics Conference on High Energy Physics, Brighton (UK), 20-27 July, 1983*, p. 216.
[124] Jonker M. *et al.*, *Phys. Lett. B*, **99** (1981) 265.
[125] Bosetti .P. C. *et al.*, *Nucl. Phys. B*, **217** (1983) 1.
[126] Shaevitz M., *Proceeding of 1981 International Conference on Physics and Astrophysics, Hawaii, 1981* Vol. **1**, p. 311.
[127] Jones G. T. *et al.*, *Phys. Lett. B*, **178** (1986) 329.
[128] Steinberger J., *Experiments with High Energy Beams*, Nobel Lectures, Dec. 8, 1988.

[129] Swartz M. L., *Precision electroweak Physics at the Z*", in *XIX Symposium on Lepton and Photon, Stanford University, August 1999*; Drees J., Contribution to Lepton Photon Conference, Rome, 2001.
[130] Denegri D., *Phys. Rep.*, **403** (2004) 107.
[131] Young R. D. *et al.*, *Phys. Rev. Lett.*, **99** (2007) 122003.
[132] Beringer J. *et al.*, *Phys. Rev. D*, **86** (2012) 010001.
[133] Baak M. *et al.*, arXiv, hep-ph (2012) 1209.2716v2.